



Technical Articles

- Observation of a Novel Physical Phenomenon in SQUID Based TDEM System for Geophysical Applications

Young Officer's Forum

- Effect of Morphological Parameters in Determining The Actual Size Distributions and Estimation of Suspended Sodium Aerosol Dynamics Pertaining to SFR Safety

Young Researcher's Forum

- Influence of B-site cation disorders on the physical properties of Gd₂CuTiO₆ with orthorhombic distortions

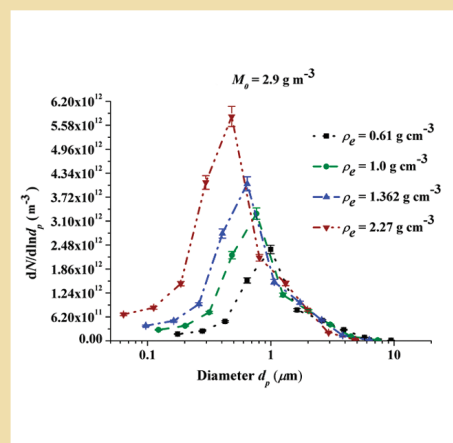
Homage to Dr. Cherian K. Mathews

News and Events

- Technology Transfers Facilitated by Incubation Centre, IGCAR
- Workshop on Electromagnetic Nondestructive Evaluation
- Sodium Charging in Sodium Technology Complex
- Theme Meeting: Radiation Metrology and National Standards for Ionising Radiation
- Inauguration of Facilities by Dr. A. K. Mohanty, Chairman, AEC & Secretary, DAE
- Signing of MoU between IGCAR and M/s. Sree Maruthi Marine Industries Limited
- Workshop on Geospatial and Radar Technologies for Improved Weather Modelling and Effective Disaster Management (GRADM 2024), IGCAR
- Celebrating Nature at IGCAR: World Environment Day, 2024

Awards, Honours and Recognitions

Bio-diversity @ DAE Campus, Kalpakkam





Editor's Desk

*Dear Reader**Greetings*

It is my pleasant privilege to forward the latest issue of IGC Newsletter (Volume 140, July 2024, Issue 2). I thank my team for their timely inputs, cooperation, and support in bringing out this issue.

The technical article of this issue "Observation of a Novel Physical Phenomenon in SQUID Based TDEM System for Geophysical Applications" is by Dr. R. Nagendran and colleagues from SAS/SDTD/MSG, IGCAR.

Young Officer's Forum features an article on "Effect of Morphological Parameters in Determining The Actual Size Distributions and Estimation of Suspended Sodium Aerosol Dynamics Pertaining to SFR Safety" by Mrs. Usha Pujala from HSEG, SQRMG, IGCAR.

The article on "Influence of B-site cation disorders on the physical properties of Gd_2CuTiO_6 with orthorhombic distortions" by Ms. Papiya Saha, SRF from CMPD, MSG, IGCAR is categorised as this issue's Young Researcher article.

Homage to Dr. Cherian K. Mathews, Former Director, Chemistry Group, IGCAR.

In the back cover, we have Red-necked falcon found in IGCAR-campus.

The Editorial Committee would like to thank all the contributors. We look forward to receiving constructive suggestions from readers towards improving the IGC Newsletter content.

We express our deepest gratitude to Director IGCAR for his keen interest and guidance.

Shri J. Rajan

With best wishes and regards

Chairman, Editorial Committee, IGC Newsletter and
Head, Scientific Information & Networking Division, IGCAR



Observation of a Novel Physical Phenomenon in SQUID Based TDEM System for Geophysical Applications

TDEM (Time Domain Electro-Magnetic) is one of the popular electromagnetic techniques widely used in geophysical exploration applications. The use of SQUIDs in TDEM geophysical exploration applications has several advantages as compared to the conventional induction coil based measurements, such as high sensitivity, wide bandwidth and wide dynamic range. SQUIDs can measure the magnetic field, B directly, whereas the induction coil measures the induced voltage which is proportional to the rate-of-change of magnetic field, dB/dt . The voltage signal from the induction coil, therefore, decays much faster and reaches the noise floor more quickly compared to the decay of the magnetic field itself, which can be directly measured if a sensitive magnetic field sensor such as SQUID is available. Therefore, the use of high sensitivity B-field sensor such as SQUID enables measurement of decay curves to be extended to later instants of time, and thereby provides better target resolution and larger investigation depth.

Working principle of TDEM

The basic principle of TDEM involves the induction of eddy currents in the sub-surface structures of earth with suitable electromagnetic excitation and subsequent measurement of the decay of these eddy currents using a suitable sensor in time domain. The typical sequential instances involved in TDEM technique are eddy current excitation in the ground by applying primary magnetic field and the decay of the induced eddy current generates secondary magnetic field are measured either by SQUID or induction coil. In this process, the net magnetic field measured with time should never theoretically reach negative values. The occurrences of sequential instances and measurements performed using induction coil and SQUID are shown in Fig. 1.

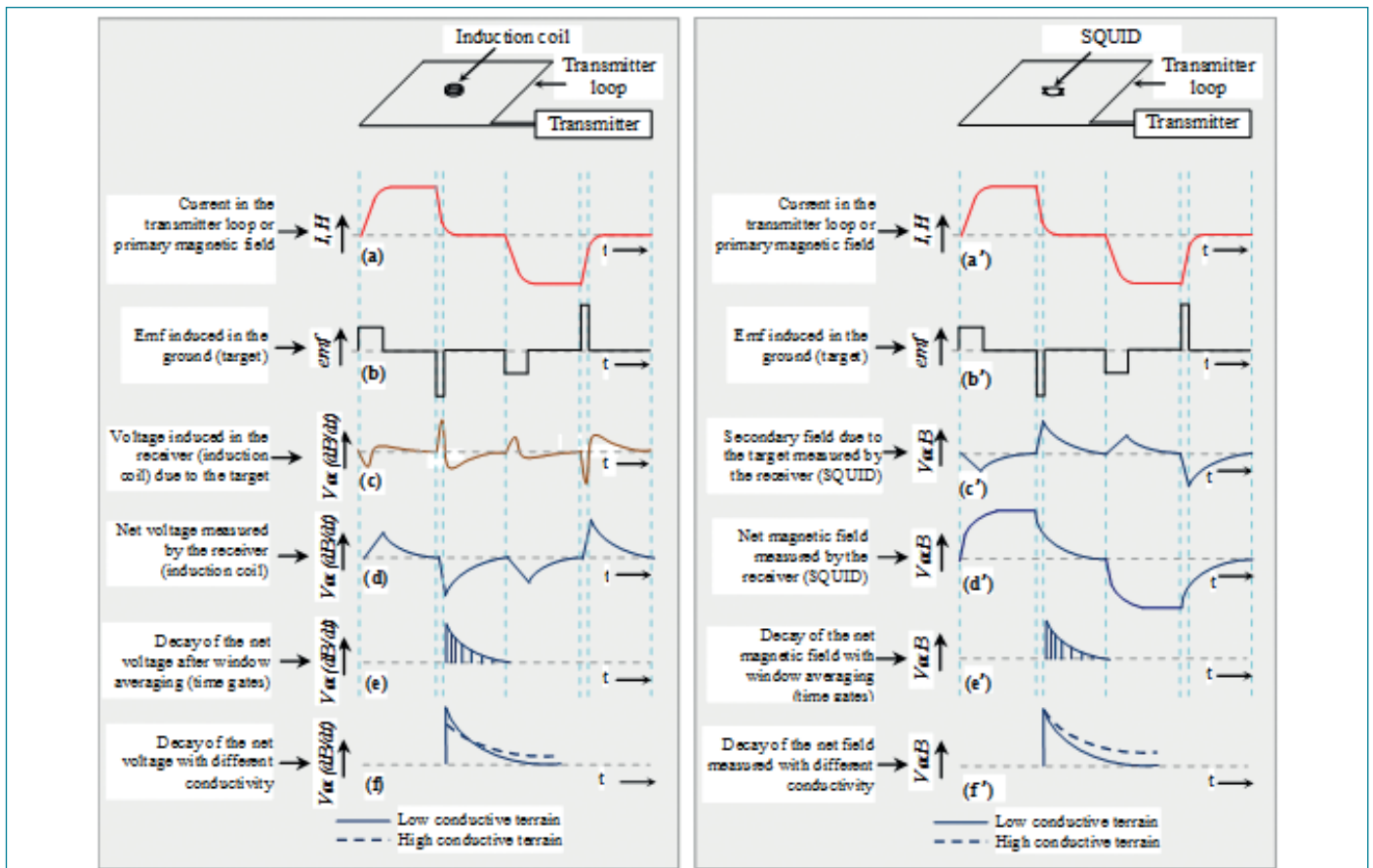


Figure 1: Schematic illustration of typical TDEM waveforms expected using an induction coil and SQUID as a receiver.

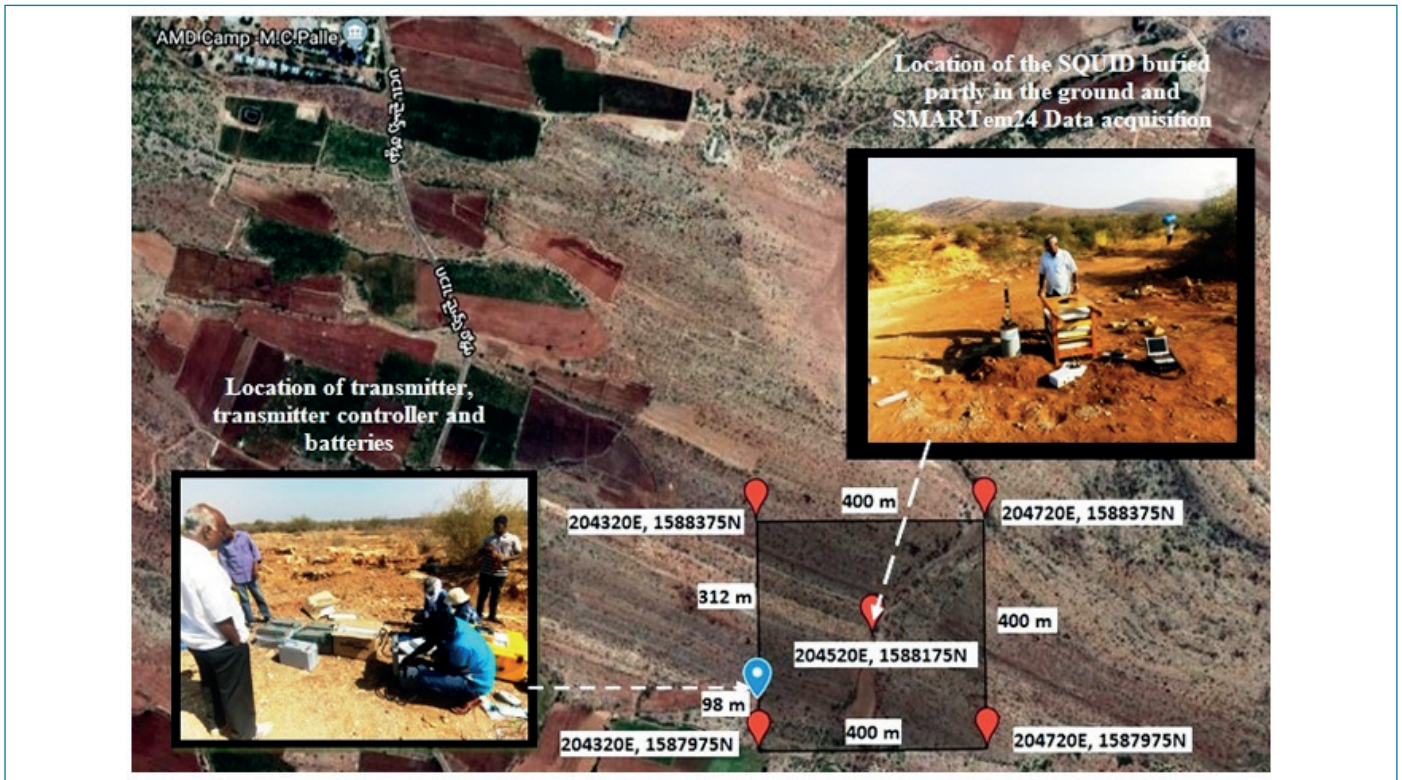


Figure 2: Photograph of the experimental site (UTM zone: 44 P: 204320E: 1587975N) along with the coordinates of the 400 m x 400 m transmitter loop and the experimental setup.

TDEM measurements with SQUID

Since the SQUID has several advantages to use as a receiver in geophysical TDEM measurements, a SQUID based TDEM system has been developed with low Tc SQUID and the system has been utilized in a terrain, where a thin conducting layer buried under thick highly resistive layer. Our very first TDEM central loop sounding measurements in the field have been performed near Tummalapalle, Cuddapah (district), in Andhra Pradesh, India in 2019. This place was chosen based on prior information regarding the lithological structure of the region. In this work, SQUID based TDEM central loop sounding measurements have been carried out with transmitter loops of different sizes. The photograph of the experimental site along with the coordinates of the 400 m square transmitter loop and the experimental setup have been shown in fig. 2. The decay of the secondary magnetic field recorded by the SQUID with different base frequencies for the transmitter loop size of 100 m x 100 m and 400 m x 400 m are shown in fig. 3 (a) and (b) respectively. In case of fig 3 (b), the response of the ground recorded by the SQUID with transmitter loop size of 400 m x 400 m and with transmitter current of 27 A show excellent resolution of the conductive layer as compared to the transmitter loop size of 100 m x 100 m with transmitter current of 25 A. Nevertheless, in these measurements, it was

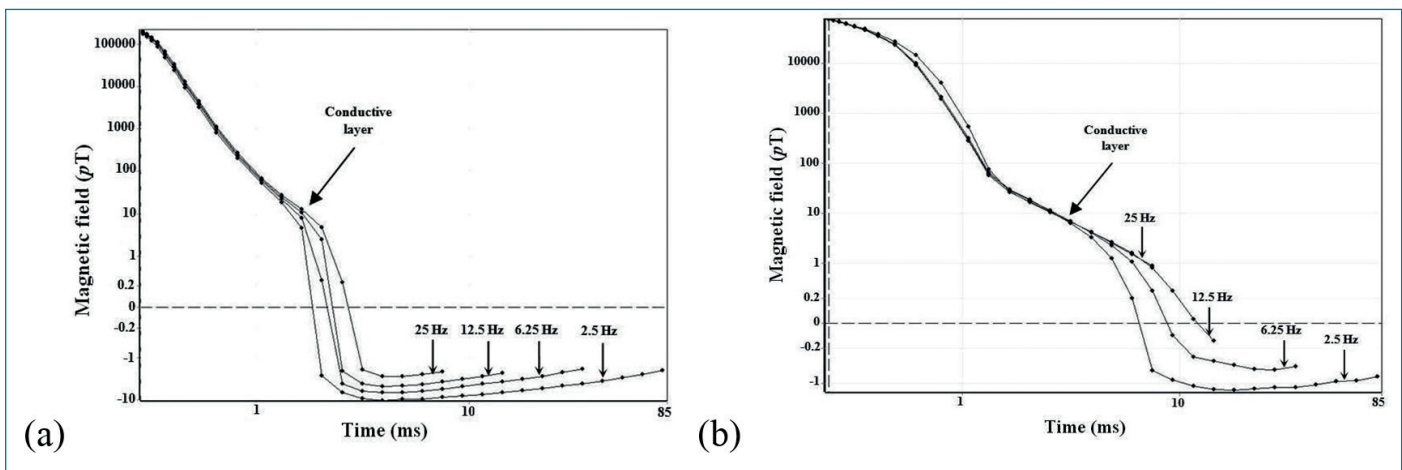


Figure 3: Decay transient recorded by SQUID (log-log scale) with different base frequencies with transmitter loop size of (a) 100 m x 100 m and (b) 400 m x 400 m.

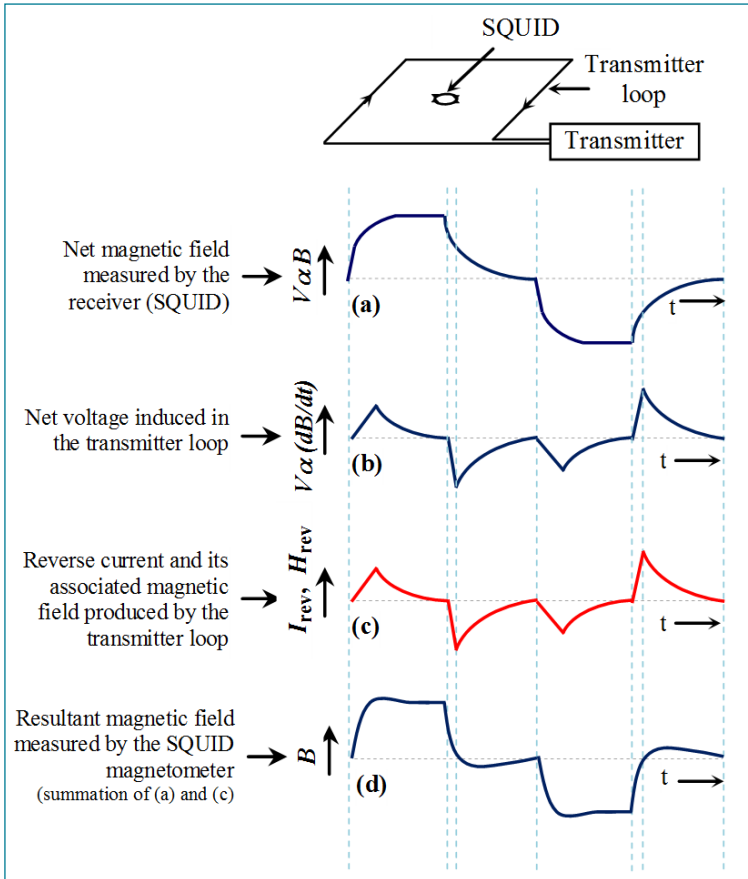


Figure 4: Schematic illustration of decay transient waveforms expected using SQUID as a receiver when effects of tertiary magnetic field produced by the transmitter loop are taken into account.

response. At a very first level of discussion, the additional magnetic field coupled to the SQUID magnetometer is described schematically with typical TDEM waveforms given in fig. 4. Here, it is assumed that the transmitter loop which is used to induce eddy currents in the target is also acting as a receiver loop. When the transmitter current is switched off, voltage induced in the transmitter loop is due to the net changes of magnetic field (primary and secondary magnetic field). Therefore, the net induced voltage $V(t)$ and its associated current flows in the transmitter loop $I(t) = V(t)/Z$. Where, Z is impedance of the transmitter loop. This induced current and its associated magnetic field also coupled to the SQUID magnetometer. In fig. 4 (a) and (b) are the expected net magnetic field measured by the SQUID magnetometer and net voltage induced in the transmitter loop respectively. Fig. 4 (c) is the equivalent current which flows in the transmitter loop and its associated magnetic field. The additional magnetic field produced by the transmitter loop is further added with the net magnetic field measured by the SQUID (fig. 4 (a)), the resultant magnetic field will reach to negative values and the same is shown in fig. 4 (d). In general, the sensitivity of

observed that the decay of the secondary magnetic field always reached negative values (zero crossover) at later decay times and the observed decay transients were found to be strongly dependent on the base frequency of the transmitter current. Similar zero crossover effects and frequency dependent TDEM transient responses have been observed with SQUID based central loop TDEM measurements by various other researchers worldwide for more than last two decades. These negative decay transients were routinely attributed to various other effects, mainly, to Induced Polarization (IP) causes erroneous results while modeling the data to obtain the geological information of the ground. But we argue that the reason for observation of the zero crossover or negative decay in central loop TDEM measurements with SQUID is attributable to the magnetic field generated by the flow of reverse current in the transmitter loop.

Novel hypothesis for the occurrence of sign reversal in SQUID based TDEM

We proposed a novel hypothesis that the occurrence of sign reversal in SQUID based TDEM central loop measurements is the flow of reverse current in the transmitter loop and its associated tertiary magnetic field coupling to the SQUID (receiver) along with the target

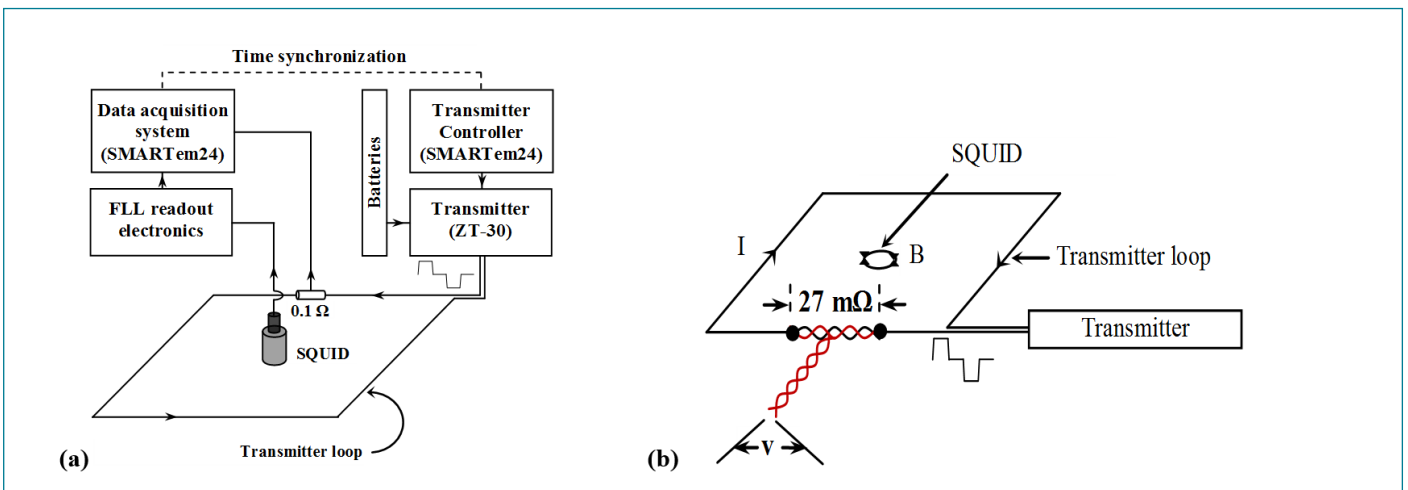


Figure 5: The schematic view of the transmitter loop (a) 100 m x 100 m and (b) with a resistor connected in series in order to measure the reverse current flow in the transmitter loop.

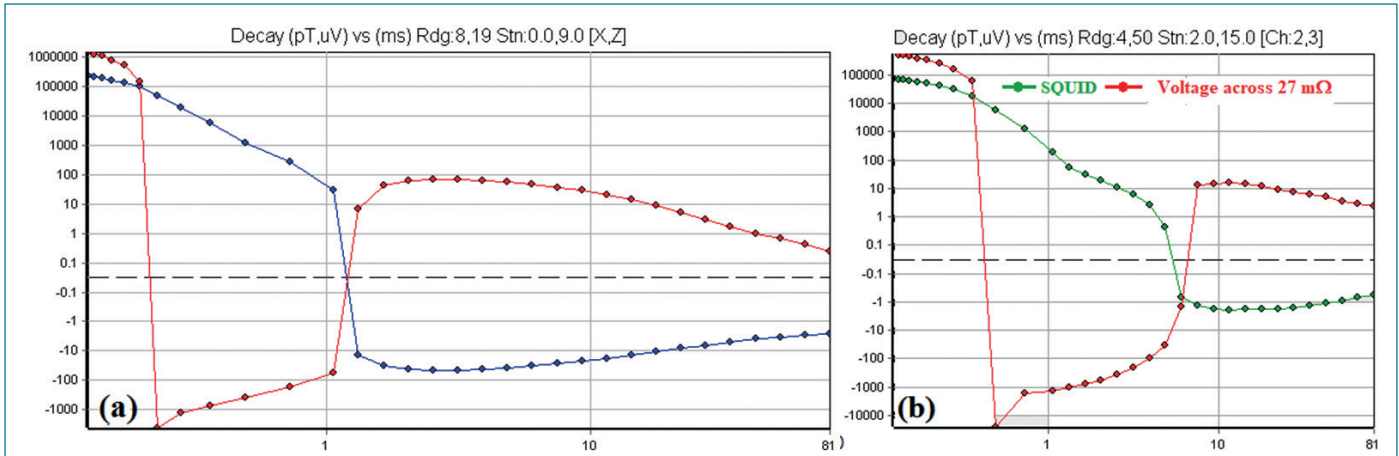


Figure-6: The recorded decay transients with SQUID at the centre of the transmitter loop and the voltage measured across the resistor connected in series with the transmitter loops of (a) 100 m x 100 m and (b) 400 m x 400 m.

the SQUID based TDEM system in time domain is around 0.01 to 0.1 pT/A after data processing including stacked and window (time gates) averaging. Therefore, the induced current of just 1 mA in the transmitter loop with size of 100 m x 100 m produces magnetic field of about 11 pT at its centre. This magnetic field is very large as far as the sensitivity of the SQUID is concerned.

The flow of reverse current in the transmitter loop has been confirmed by repeating the central loop TDEM measurements at the same place with an additional provision to measure the instantaneous current flowing through the transmitter loop and simultaneously measure the decay of the secondary magnetic field using SQUID sensor located at the centre of the transmitter loop. A transmitter loop in the form of a square with side length of 100 m, in which a resistor with a value of 0.1 Ω is connected in series with the transmitter. The SQUID sensor, which measures the vertical component of the magnetic field, is located at the centre of the transmitter loop. A wire in the form of a twisted pair is used to measure the voltage drop across the 0.1 Ω resistor. The twisted pair from 0.1 Ω resistor has been brought to the centre of the transmitter loop in order to measure the SQUID output and the voltage across 0.1 Ω resistor by keeping the data acquisition system at the same place. The SQUID measures magnetic field in units of pT and the voltage across the 0.1 Ω is measured in units of μV. The experiments have been further repeated for the transmitter loop with a side length of 400 m. In this experiment, a small part of the transmitter loop itself is used as a resistor and the voltage drop across this resistor is measured against time. The part of the transmitter loop whose length is about 11 m is used as a resistor. The dc resistance of the wire is about 27 mΩ which is independently measured in the laboratory by four probe method. The schematic view of the transmitter loops with a resistor connected in series, across which voltage is measured, are shown in fig. 6. The recorded output of the SQUID located at the centre of the transmitter loop and voltage measured across the resistors for both transmitter loops are shown in fig 7. This experimental data with larger transmitter loop clearly indicates that the SQUID is sensing the ground response in addition to the reverse current flow in the transmitter loop. This unwanted flow of reverse current destroying the signals at later times which are coming from the deep layers of the ground. The secondary magnetic field produced either due to inductive current or polarized current from the ground should provide a response in such a way that the voltage induced in the transmitter loop decays much faster than the decay of the magnetic field which is directly measured by the SQUID. But, from fig. 7 the time at which the occurrence of sign reversal is same. This clearly indicates that the SQUID is measuring the flow of reverse current induced in the transmitter loop and not the magnetic field responsible for the induced polarization phenomenon.

The experimental results and analyses provide credible evidence to explain that the sign reversal effects in SQUID based TDEM measurements are not parasitic effects of an unknown origin, but represent real physical phenomena involving the flow of induced current in the transmitter loop which is responsible for the tertiary magnetic field generation in TDEM. To elucidate the underlying phenomena, suitable methodologies have to be devised either to eliminate or minimize such induced reverse current flows in the transmitter loop in order to get the genuine transient response of the target which provides appropriate geological structures through suitable modeling.

*Reported by
Dr. R. Nagendran and colleagues
Materials Science Group*



Young Officer's Forum



Mrs. Usha Pujala completed her M.Sc (Space Physics) from Andhra University, Visakhapatnam in 2008 and joined in DAE through 53rd batch of training school in 2009. She joined RESD, IGCAR in 2010. She completed her M. Tech in Nuclear Engineering in 2013 from HBNI. Her research interests are studies on aerosol issues pertaining to fast reactor safety and associated nuclear fuel cycle facilities. She has completed PhD and submitted the thesis titled "Effect of aerosol morphology and charging over the dynamics of aerosols in a closed chamber in the context of Sodium cooled Fast Reactor (SFR) safety analysis" to HBNI. Presently, she is working as SO/F at HISD/SQRMG, IGCAR.

Effect of Morphological Parameters in Determining The Actual Size Distributions and Estimation of Suspended Sodium Aerosol Dynamics Pertaining to SFR Safety

Evaluation of properties and concentration decay of suspended aerosol inside the Reactor Containment Building (RCB) with time is critical to estimate the Environmental Source Term (EST) due to the release of radioactive material from various RCB leak paths during hypothetical Core Disruptive Accident conditions (CDA) of SFR. Sodium combustion aerosol is in the micrometer size range, and its initial mass concentration M_0 envisaged for Prototype Fast Breeder Reactor (PFBR) during CDA conditions is 4 g/m^3 . The aerosols of fission products and fuel materials of the core generated by vaporization and condensation in RCB are in the sub-micrometer size range, and their estimated total concentration M_0 is about $\sim 40 \text{ mg/m}^3$. The sodium and core material aerosols of SFR are porous and non-spherical with distinct morphological properties.

Mechanistic models considers the dominant sodium aerosol alone to evaluate the deposition rates of aerosols in RCB as it co-agglomerate with core material aerosols and deposit. Owing to the common mass based measurements of sodium aerosol using impactor techniques, models use either a single representative mass median diameter (MMD) or size distribution from the experimental data available in the open literature. Further, models assume that the particles as rigid spheres (dynamic shape factor $\chi=1$) with material and particle densities are equal ($\rho_p=\rho_m$) or applied with conservative density correction factor α of 0.5 ($\rho_e=0.5*\rho_m$). Also, constant size-independent diffusion boundary layer thickness (δ) in the range of 10 to 100 μm is considered in the models. However, actual initial aerosol number size distributions corrected with effective density (ρ_e), shape factor χ , and the particle size dependent δ values should be incorporated in the model for the realistic estimation of coagulation and deposition processes in the early phases of the sodium fire as the particles will be in the sub-micrometre size range. In this context, studies are carried out in a 1 m^3 test chamber at the Aerosol Test Facility (ATF). Morphological parameters and effective density corrected initial number size distributions of sodium aerosol are determined. A polydisperse aerosol dynamics model is developed and validated with test chamber experiments. The validated parameters are used for predicting the sodium aerosol concentration decay inside RCB of PFBR during CDA.

Morphological properties of sodium aerosol

The morphological properties of sodium aerosols are measured using real-time MASTERSIZER - QCM techniques. Parallel measurements of different equivalent diameters are used to derive the average χ and ρ_p values of aerosol at three different RH conditions 75%, 55% and 30% RH. It is observed that sodium aerosol particles are porous due to agglomeration process and hence ρ_p is much lesser than ρ_m values. The properties change with time and tend to reach saturation value. The ρ_p values are observed to vary in the range of 1.5 ± 0.15 to $1.9 \pm 0.21 \text{ g/cm}^3$ at various time periods during the test with 75% RH and its average value is $1.67 \pm 0.41 \text{ g/cm}^3$. Similarly, the ρ_p values averaged over the entire period at 55% and 30% RH conditions are 1.43 ± 0.36 and $1.2 \pm 0.31 \text{ g/cm}^3$, respectively. The carbonation process is faster at higher humidity conditions, and hygroscopic growth is more. Also the pores of the agglomerated particles get filled

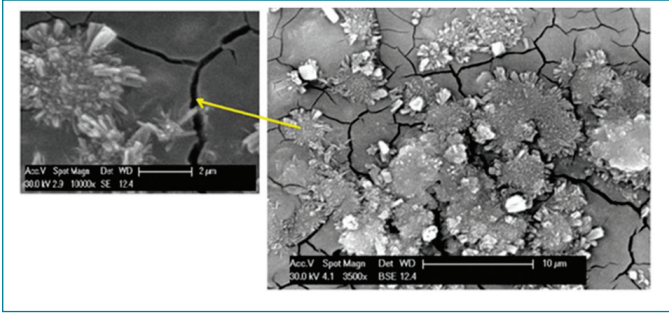


Figure 1. SEM micrograph of sodium aerosol at 55 % RH.

to have a slight deviation from spherical shape, and the particles are expected to be in cubical to cylindrical forms. The ρ_e value at 55% RH is about 1.36 g/m³, significantly less than the material density of sodium oxide species, 2.27 g/cm³.

Details of nodal-method based aerosol dynamics model

Based on the nodal method, a poly-disperse aerosol dynamics code is developed to model the suspended aerosol concentration decay and size growth with time inside the test chamber. The respective general dynamic equation solved by the nodal method is given in Eq-1.

$$\frac{dN_k}{dt} = \frac{1}{2} \sum_{i=1}^{max-1} S_{ijk} K_{ij} N_i N_j - N_k \sum_{i=1}^{max-1} K_{ik} N_i - \beta_k N_k \quad (1)$$

Here K_{ij} is the collision frequency function between the particles of nodes i and j . S_{ijk} is the size splitting factor. The suspended aerosol behavior is simulated from the completion of generation by defining the initial aerosol number size distribution, along with morphological parameters of the particles. The Brownian

coagulation and kinematic coagulations owing to gravitational, turbulent, and electrostatic forces are considered. The electric forces are due to the charge levels of particles obtained from generation process. The deposition due to gravitational settling, diffusive deposition, and thermophoresis are accounted for in the model. Particle size-dependent diffusion boundary layers δ are incorporated. The particle loss due to the sampling of aerosols for measurements is accounted by defining the average sampling loss rate.

Validation with PAO aerosol dynamics in test chamber

Real-time number concentration decay and size growth of PAO aerosol suspended inside the chamber measured using ELPI is used to validate the model. Measured initial PSDs of PAO aerosol with respect to two densities i.e., $\rho_0=1.0$ g/cm³ (reference aerodynamic), and $\rho_e=0.82$ g/cm³ (the actual density of PAO oil drop) measured using ELPI are shown in Fig. 2. The size distributions corresponding to the densities of 1.0 and 0.82 g/cm³ are called Aerodynamic Particle Size distribution (APSD) and Mobility Equivalent Particle Size Distribution (MEPSD), respectively. PAO aerosol distribution is a single mode. The APSD has a total concentration of 1.63×10^{12} /m³, Count Median Aerodynamic Diameter (CMAD) of 0.315 μ m and asymmetric with an average σ_g of 1.86. The MEPSD has a total concentration of 1.38×10^{12} /m³, Count Median Mobility Equivalent Diameter (CMMED) of 0.35 μ m, and asymmetric with an average σ_g of 1.845. As the actual ρ_e value of PAO particles is lesser than 1 g/cm³, the MEPSD gets shifted to the higher size axis compared to APSD, resulting in the CMMED more than CMAD. This is based on the equivalent diameter concept with equal terminal gravitational settling velocities. The difference between APSD and MEPSDs increases if the ρ_e of aerosol is much differed from 1 g/cm³. PAO aerosol is almost neutral, and the average number of charges per particle acquired during generation by atomization process j_{av} is only 0.02 ± 0.01 . The value of 0.02 is used to model the electrostatic coagulation, considering that all the particles have the same net charge independent of size.

The number concentration decay and size growth modeled in two test cases using APSD and MEPSD are shown in Fig. 3. From the detailed sensitivity analysis, it is observed that Brownian coagulation is the predominant contributor to aerosol dynamics, followed by gravitational settling and sample loss for measurements with the given experimental conditions. Diffusive deposition contribution is within 1% under natural convective conditions in closed confinement. The net charge level of PAO aerosol obtained from generation is insignificant and does not cause enhancement in Brownian coagulation. Overall, the sensitivity analysis carried out for PAO aerosols shows that

with more moisture at high humidity levels. This phenomenon could increase the particle density to some extent at higher humidities. The sodium aerosols become more porous at lower humidity conditions & pores could be filled with air. The average shape factors χ of sodium aerosol measured at 75%, 55%, and 30% RH are 1.05 ± 0.13 , 1.05 ± 0.13 , and 1.07 ± 0.13 , respectively. The derived shape factors represent that the particles are nearly spherical at 55% and 75% RH, as the initial sodium compound aerosol is in colloidal form and take the spherical shape, as shown in the SEM micrograph of Fig.1. The derived shape factors at 30% RH are found

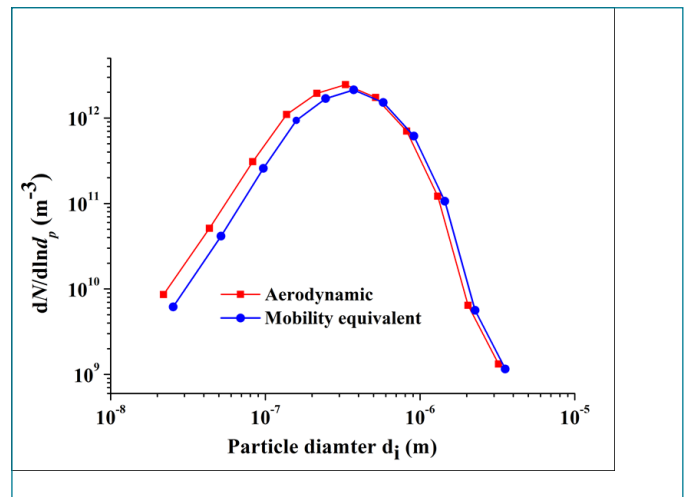


Figure 2: Initial equivalent size distribution of PAO aerosol

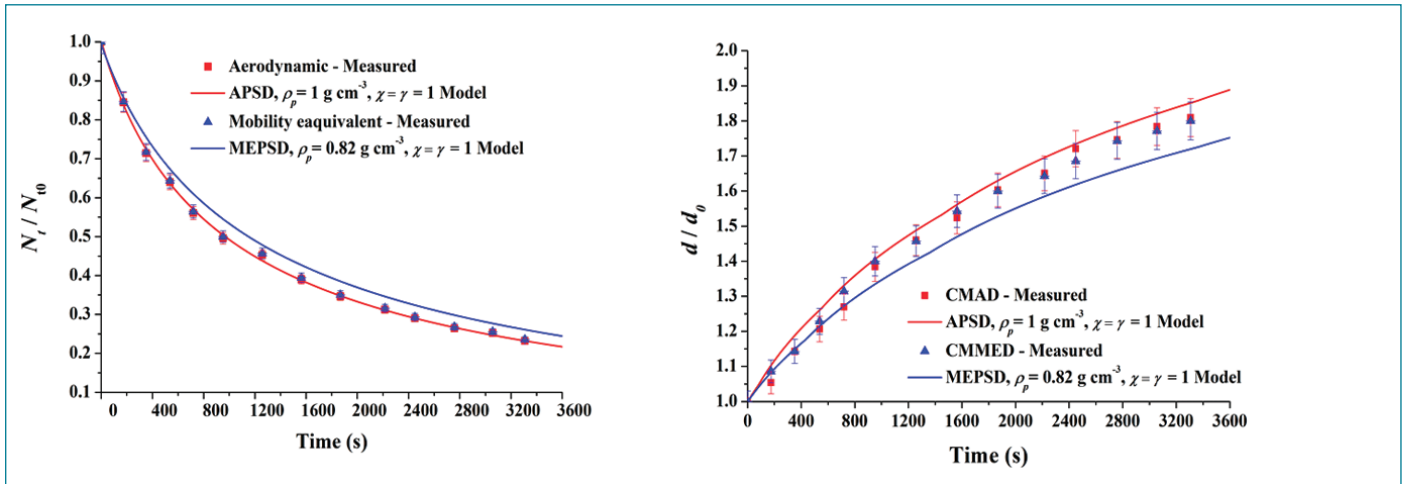


Figure 3: Measured and modeled PAO aerosol concentration decay (left), size growth (right).

- i) The difference in effective densities 0.82 and 1 g/cm³ causes marginal differences among the aerodynamic and mobility equivalent PSDs about 11% in initial median diameters and 15.3% in total concentration.
- ii) Both the APSD and MEPSDs satisfactorily simulate the aerosol dynamics within 1 to 10% compared to corresponding measurements for the spherical, non-porous PAO aerosols as particle density is not much different from 1 g/cm³.
- iii) For a given PSD, the density of either 1 or 0.82 g/cm³ used to model the aerosol processes does not significantly affect the predicted aerosol behavior.

Validation with sodium aerosol dynamics in test chamber

Sodium aerosol test is carried out at M₀ of 2.9 g/m³ at 47±3% RH. The measured initial APSD of sodium aerosol just after the completion of generation is shown in Fig. 4. The APSD is corrected with different ρ_e values to arrive the respective MEPSDs i.e. i) measured ρ_e value at ATF for M₀ of 2.0 g/m³ at 55% RH i.e. 1.36 g/cm³ (ρ_p=1.43, χ=1.05); ii) sodium oxide material density of 2.27 g/cm³ (ρ_p=2.27 g/cm³, χ=1); iii) Hinds et al. 1977 reported 0.61 g/cm³ (i.e. ρ_p=0.836 g/cm³, χ=1.37). The MEPSDs are also shown in Fig. 4. The sodium aerosol concentration increases nearly three times, and the median diameter decreases by almost half if the ρ_e increases from 0.61 g/cm³ to the material density of 2.27 g/cm³ for the given mass concentration as shown in Table 1. It is also observed that the σ_g of derived MEPSDs marginally increases with the effective density. The actual size distribution which could be among these APSD or MEPSDs could not be confirmed directly. So this study performed analytical tasks using four types of distributions and the corresponding morphological parameters listed in Table 1 and analyzed for realistic estimates to ascertain actual size distribution and morphological parameters.

The sodium aerosol generated by combustion is highly charged compared to the standard PAO aerosols generated by atomization. The sodium aerosol of size < 1 μm is dominantly negatively charged with a maximum number of charges up to -15. The particles > 1 μm mostly contain a net positive charge. The representative average number of charges per particle j_{av} of -3.3 (averaged over entire size distribution) is used to model the electrostatic coagulation by considering that j_{av} is the same for all the particles independent of size. The patterns of measured and modeled concentration decay and size growth with time of the tested cases are compared up to 4400±10 s in Fig. 5.a and b. It is to be noted that for the verified four sets of PSDs and corresponding morphological properties, the gravitational settling rates are the same based on the equivalent diameter concept. Diffusion, thermophoresis, and electrostatic coagulation processes are insignificant within 2%. The effect of sample loss for the measurements is significant up to 5%. The sample removal rate is the same for the four model cases in a given test, and hence the effect is the same. Therefore, the Brownian coagulation mainly differed by changing the equivalent size distributions.

The MEPSDs correspond to ρ_e of 2.27 g/cm³ i.e. T1MC4 case of Table 1 overestimates the coagulation as the particle sizes are significantly smaller than actual. This causes a larger deviation of about 40% for number concentration decay and around 28.7 to 33%

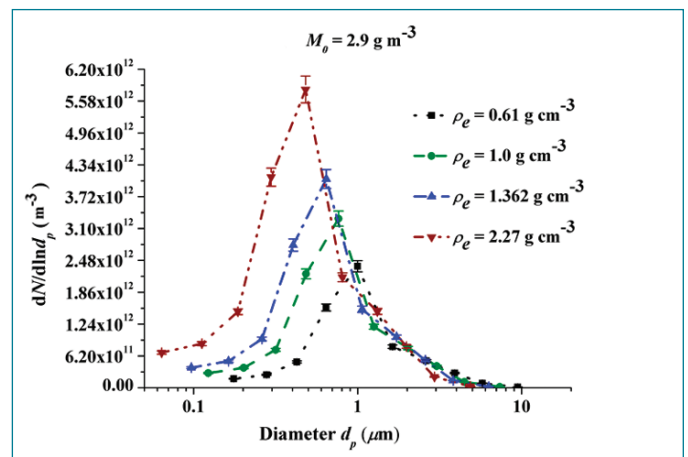


Figure 4: Equivalent initial number size distributions of sodium aerosol at various effective densities.

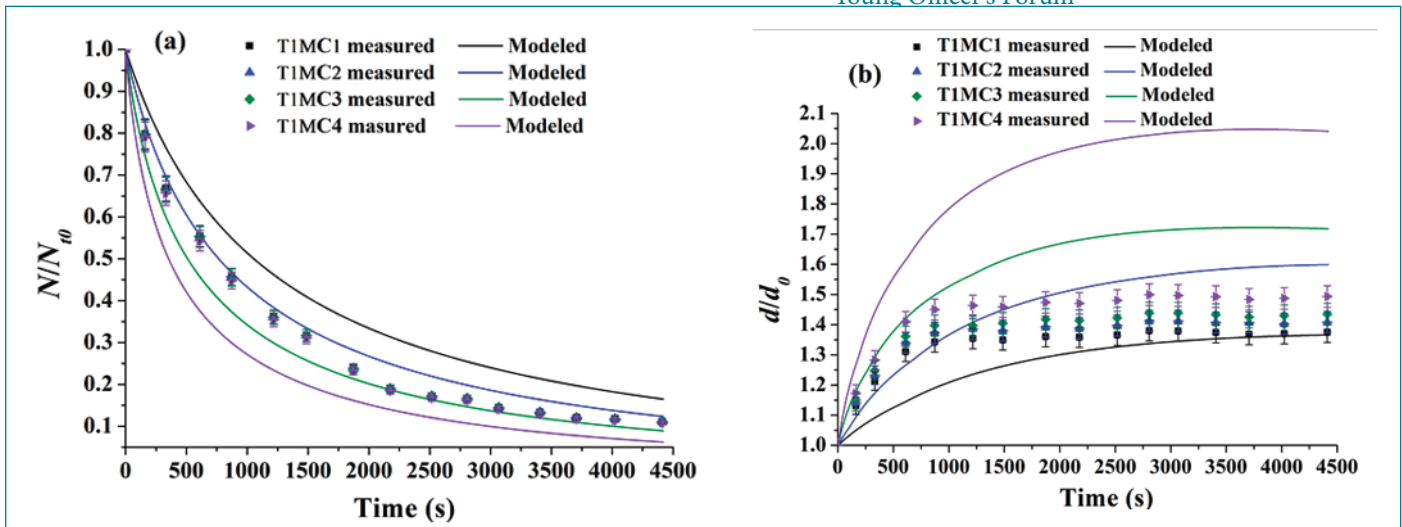


Figure 5: Measured and modeled sodium aerosol a) concentration decay (top), b) size growth

for size growth. Both the aerodynamic and mobility equivalent PSDs of $\rho_p=1 \text{ g/cm}^3$, $\chi=1$; and $\rho_p=1.43 \text{ g/cm}^3$, χ of 1.05 i.e. T1MC2 and T1MC3 cases provided the best agreement between the measured and modeled dynamics within 11.1% to 15.45% for number concentration decay and 11.5% to 17.5% for size growth respectively. Here, the aggregation enhances the more porous nature of the particle. Further, the pores of the particles get filled with moisture and tend to become colloidal, and this causes a reduction in the actual density of particles from material density by the time of completion of generation itself.

The validation process is also carried out for the sodium aerosol tests with initial mass concentrations of 0.1 and 1.0 g/m³. At the low initial concentration 0.1 g/m³, the aggregation of particles is feeble to cause porous nature, which may lead to particle density nearer to material density, and hence the PSD corresponding to density of 2.27 g/cm³ caused the best agreement. At sufficiently high concentration 1.0 g/m³, the PSD corresponds to $\rho_e = 1 \text{ g/cm}^3$, giving a better match within 11 to 18% due to enhanced aggregation process causing a more porous nature to the particle.

Literature shows that the sodium aerosol mass size distributions measured by impaction/centrifuge separation based techniques during generation or early periods after the completion of sodium fire are of micrometer sized (MMD of 0.85 to 5.5 μm) and highly polydisperse (σ_g of 1.4 to 3). The respective number size distributions get shifted to lower particle sizes compared to the equivalent mass size distributions with the count median size (CMD) of about 0.2 to 0.6 μm . This shift increases with an increase in polydispersity. ELPI used in this work covers the particles in the larger size range from 0.01 to 10 μm and measure in real-time. The size distribution measured just after reaching the target concentration of 2.9 g/m³ has the median size CMAD of $0.66 \pm 0.1 \mu\text{m}$ and σ_g of 1.96. This is equivalent to MMAD of 2.6 μm which is in line with the literature reported micrometre size particles determined from mass based measurements.

Modelling of suspended mass concentration of sodium aerosol inside RCB

The validation of nodal code and the ascertained aerosol properties CMD of 0.66 μm and σ_g of 1.96 are further extended by simulating the

Table 1. Properties of initial equivalent PSDs of sodium aerosol					
Mass Conc. (M ₀) (g/m ³)	ρ_e (g/cm ³) i.e., ρ_p (g/cm ³) and χ	Total number conc. N ₁₀ (x10 ¹⁰ /m ³)	Initial CMAD or CMMED d ₀ (μm)	Average initial σ_{g0}	Model case no.
2.9±0.25	0.61 (0.836, 1.37)	148±6.4	0.87±0.02	1.89	T1MC1
	1 (1, 1) (Aerodynamic)	213±9.2	0.66±0.01	1.96 ($\sigma_{g1}=1.80$ & $\sigma_{g2}=2.13$)	T1MC2
	1.36 (1.43, 1.05)	270±11	0.55±0.01	2.27	T1MC3
	2.27 (2.27, 1.0)	400±17	0.4±0.01	2.13	T1MC4

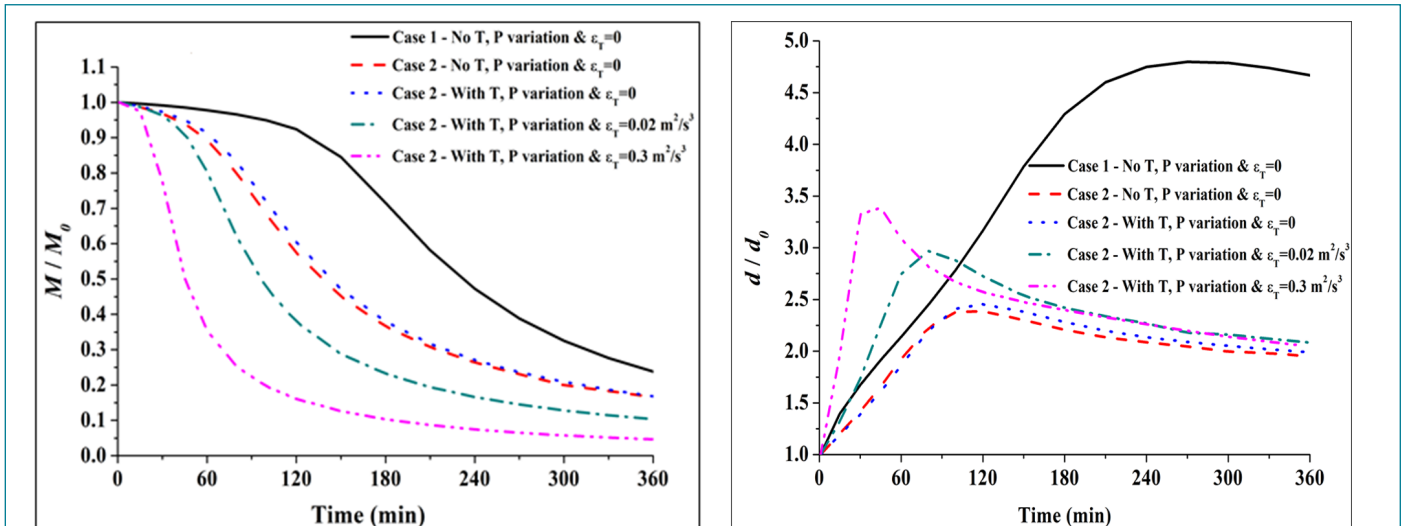


Figure 6: Modeled mass concentration decay (left) and size growth (right) of aerosol in RCB of PFBR, for the two tested PSDs with and without including temperature, pressure and turbulence effects.

mass concentration decay for the initial sodium aerosol concentration of 1.9 g/m^3 and compared with the measured and HAARM-S code modelled mass concentration decay reported in the literature for the given chamber. The suspended sodium aerosol behaviour in RCB of PFBR during CDA condition with envisaged M_0 of 4 g/m^3 , is modelled using $\text{CMD} = 0.66 \mu\text{m}$, $\sigma_g = 1.96$, $\rho_p = 1.0 \text{ g/cm}^3$ and $\chi = 1$ (case 2) as shown in Fig. 6. The homogenous concentration inside RCB and chargeless particles are assumed. Compared to the modelled behaviour using mono-disperse PSD with an MMD of $1 \mu\text{m}$, σ_g of 1.2 (case 1) reported in literature, the estimated concentration decay enhances up to the maximum of 37% within 6 hours by using the recommended PSD (case 2) due to enhanced size growth with time. The faster decay of aerosol concentration could reduce the environmental source term associated with particulates. The effect of simultaneously varying both the temperature and pressure of RCB during CDA condition is insignificant on aerosol dynamics. Turbulence (specified by parameter ϵ_T , the dissipation rate in Fig. 6) affects the coagulation significantly and enhances the concentration decay, however actual turbulence parameters are to be ascertained.

Conclusion

The input parameters, such as initial number size distribution and morphological parameters, are critical in evaluating the accidental suspended aerosol behaviour in SFR containment. This work signifies the sensitivity of sodium aerosol's effective density (ρ_e) in deriving the actual size distributions from the measured aerodynamic size distributions using impactors and realistic estimation of suspended aerosol behaviour. The polydisperse aerosol dynamics code is developed and validated with the standard (non-porous and spherical) aerosols and applied to study the dynamics of actual non-radioactive equivalent sodium aerosols envisaged in SFRs. Actual number size distribution of sodium aerosol and morphological properties are ascertained or the improved estimation of the suspended aerosol behaviour of RCB.



Papiya Saha, SRF currently doing Ph.D in Physics at IGCAR, Kalpakkam under the guidance of Dr. Nithya Ravindran. Her current research interest is the study on structure property correlation on 3d/4d transition metal ion based double perovskite systems and their related applications. She joined in CMPD, MSG as a JRF in 2019. She has completed her B.Sc. and M.Sc. in Physics with first class from University of Calcutta. She also worked as a project fellow in Jadavpur University, Kolkata on PVDF based nanocomposites for microwave absorption application and published several peer-reviewed articles. She has published eight peer reviewed research article from MSG research group.

Influence of B-site cation disorders on the physical properties of Gd_2CuTiO_6 with orthorhombic distortions

Double perovskite (DP) oxides with the general formula $A_2B'B''O_6$ are extensively investigated due to their compositional flexibility, material stability and wide range of physical properties ranging from insulating to metallic to half-metallic, antiferromagnetic to ferromagnetic to ferrimagnetic, multiferroicity, superconductivity, catalytic properties. As a result, DP is gaining great technological interest, with a range of possible applications such as dielectric materials in electronic devices and sensors, magnetic memory components, materials for solar cells etc. The electronic and magnetic properties of DP are largely governed by the transition metal ions at B sites and their ordering. Recently, extensive research is going on the miniaturization of microelectronic devices which requires dielectric materials with robust dielectric response with respect to temperature and frequency, moderate dielectric constant and low dielectric loss. In this article, we have reported the effect of the B site disorder on the structural, dielectric, magnetic and optical properties of DP, Gd_2CuTiO_6 (GCTO).

GCTO is synthesized using conventional solid state reaction route. High pure raw oxides of Gd_2O_3 , CuO & TiO_2 were measured according to the nominal composition of GCTO and mixed in an agate mortar for several hours and calcined at $900^\circ C$ for 48 hours. Finally, after the formation of single phase, powder was pressed into pellet and sintered at $1200^\circ C$ for 24 hours. Room temperature X-ray diffraction (XRD)

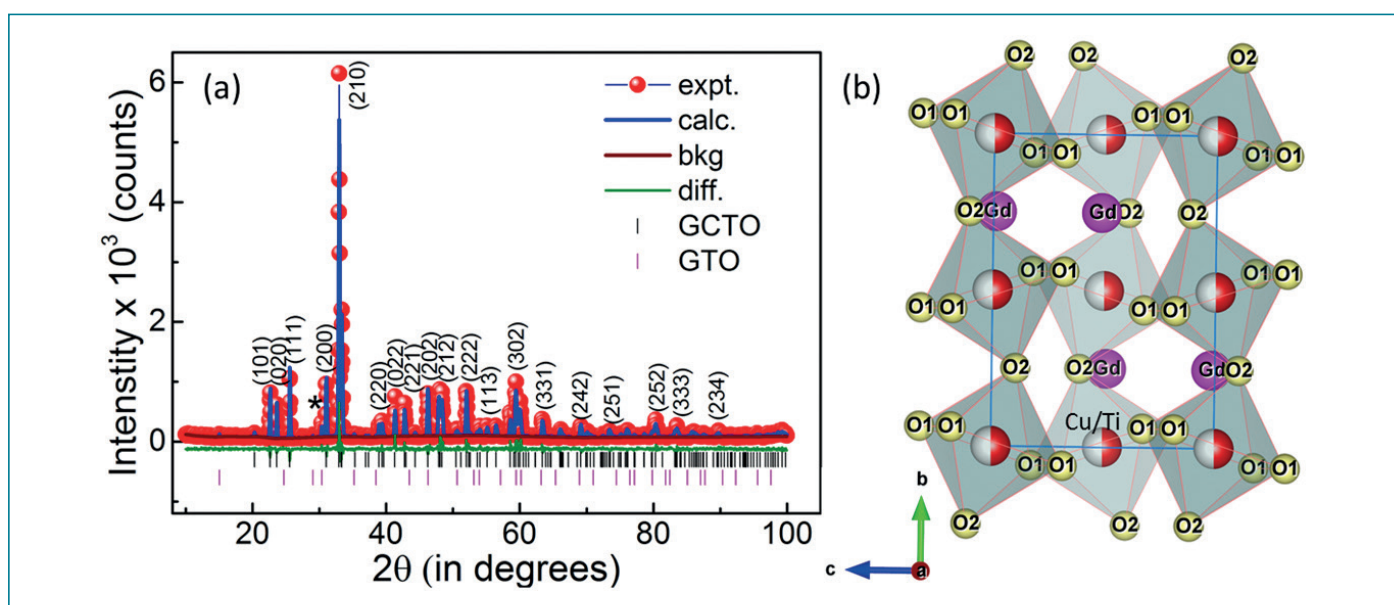


Figure 1(a) Rietveld refinement on the room temperature X-ray diffraction pattern of GCTO. Experimental (red symbol) and calculated (blue line) pattern along with the difference between them (lexpt.-lcal., shown by green line) and background (maroon line) are shown. Bragg positions for GCTO and GTO are shown by black (up) and pink (down) vertical lines. (*) symbol signifies GTO peak at 30.4° , (b) orthorhombic unit cell of GCTO.

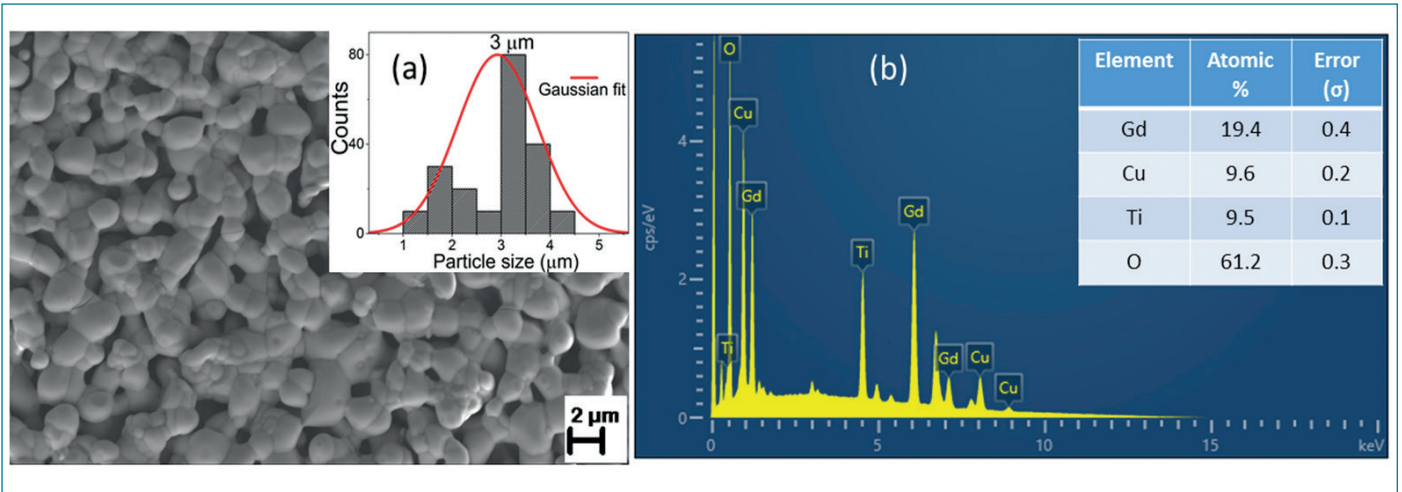


Figure 2 (a) Surface morphology of GCTO in 2 μm scale, inset: particle size distribution using Gaussian fit and (b) EDX spectrum, inset: elemental ratio (atomic %) with error (σ).

pattern of GCTO reveals crystalline nature of GCTO (Figure 1 (a)). Rietveld refinement is performed using GSAS-II software with Pnma (#62) space group and the value of χ^2 red is 2.16. The lattice parameters are $a = 5.759$ (7) \AA , $b = 7.525$ (5) \AA & $c = 5.365$ (3) \AA . No superlattice reflections are observed from the XRD pattern indicating random distribution (disorders) over the B site cations by Cu^{2+} and Ti^{4+} ions. The presence of secondary phase due to $\text{Gd}_2\text{Ti}_2\text{O}_7$ (GTO) (shown by * symbol in Figure 1(a)), is estimated to be 0.53% in GCTO. From the unit cell of GCTO (Figure 1(b)), drawn using VESTA software tilting of the Cu/Ti-O_6 octahedra along the b axis is prominent. The tilting angle

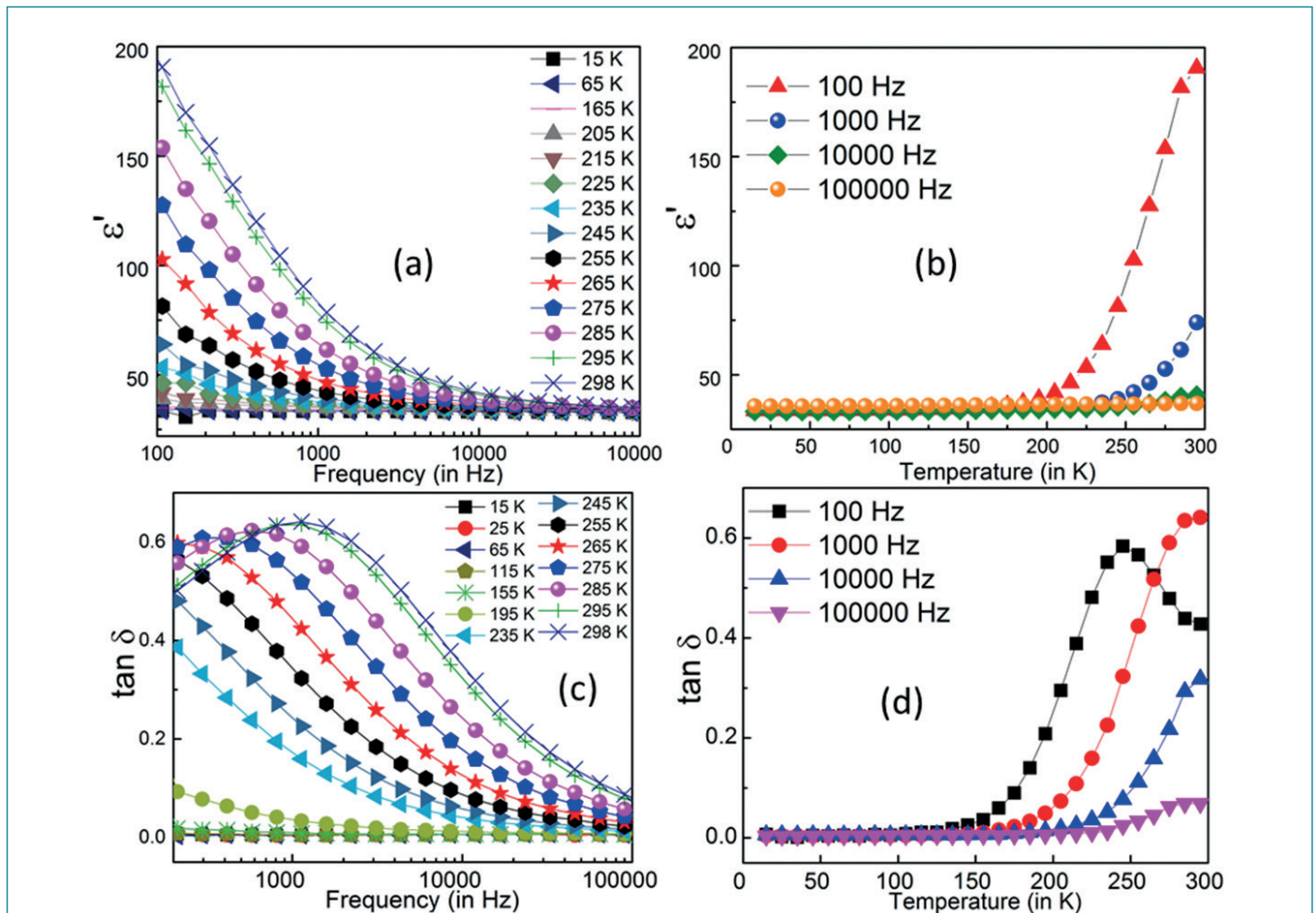


Figure 3 Variation of real part of permittivity (ϵ') (a) with frequency under several temperatures, (b) with temperature at particular frequencies, (c) variation of dielectric loss ($\tan \delta$) with frequency at different temperatures (d) variation of dielectric loss with temperature under different applied frequencies.

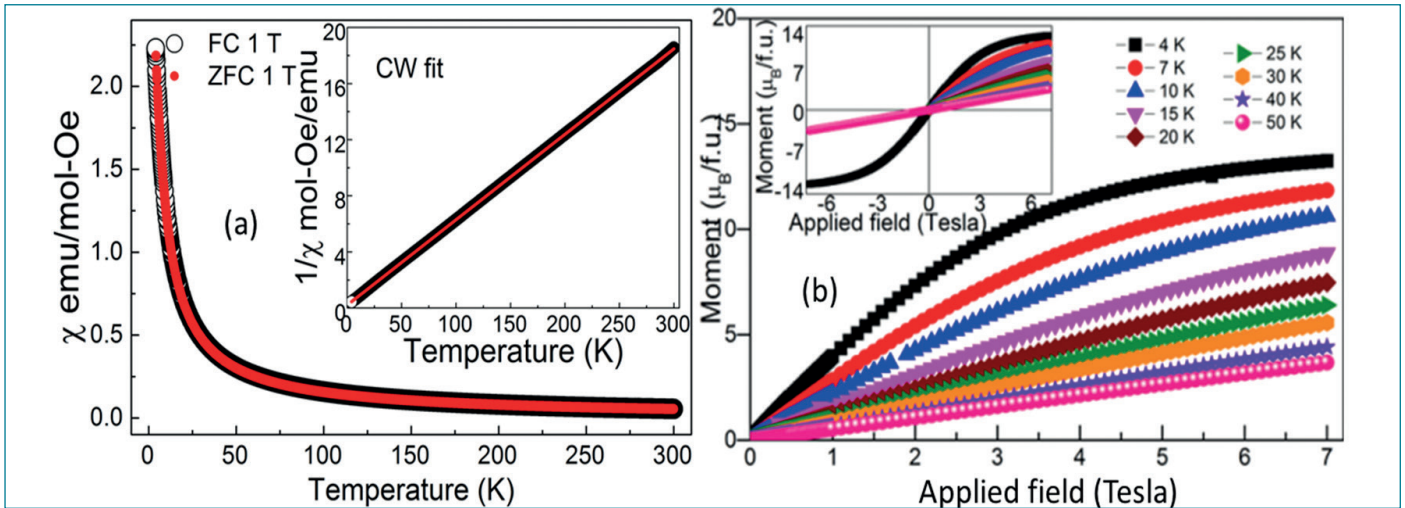


Figure 4. (a) $\chi(T)$ at 1 T applied field under FC and ZFC modes, inset: CW fit, (b) $M(H)$ curves in the first quadrant under 0 T to 7 T, Inset: $M(H)$ curves in the whole magnetic field range of -7 T to +7 T.

is 18.35° along the b axis. Distortion index (DI) of Cu/Ti- O_6 octahedra is 0.027 and bond valence sum (BVS) for Gd, Cu and Ti are 3.059, 2.305 and 3.329 respectively. From the BVS values it is inferred that Ti is under tensile strain while Gd and Cu are under compressive strain which ultimately results in orthorhombic distortion in GCTO. From the X-ray photoelectron spectroscopy the oxidation states of Gd, Cu, Ti and O are 3+, 2+, 4+ and 2-, which is consistent with the nominal composition of GCTO.

Nearly spherical dense morphology is observed from the SEM micrograph (Figure 2(a)). The average grain size of GCTO as obtained from the Gaussian distribution is $\sim 3 \mu\text{m}$. From the inset of the EDX spectrum (Figure 2(b)) the obtained ratio of the constituent elements Gd:Cu:Ti $\sim 2:1:1$ are in agreement with the stoichiometry of GCTO.

Sharp drop in the values in ϵ' with the increase in frequency (after 10 KHz) is observed from Figure 3(a) as the dipoles begin to lag behind the applied ac field at much higher frequency. $\epsilon'(T)$ (Figure 3(b)) remains constant up to a certain temperature, known as the threshold temperature, which is 200 K at 100 Hz. This threshold temperature increases with the increase in frequency. Independent (robust) dielectric response with respect to temperature and frequency is due to the disorders in the B site ($\text{Cu}^{2+}/\text{Ti}^{4+}$) cations in GCTO. Dielectric loss, $\tan(\delta)$ vs frequency (Figure 3(c)) in the temperature range 15 K - 298 K shows prominent peaks which is shifted towards the higher frequency with the increase in temperature indicating dielectric relaxation in GCTO. The dielectric relaxation present in GCTO is due to the randomness in the B site cations ($\text{Cu}^{2+}/\text{Ti}^{4+}$) and the octahedral distortion. The disorder and distortion is confirmed from the structural analysis. The variation of $\tan(\delta)$ with temperature (Figure 3(d)) under several frequencies (100 Hz, 1000 Hz, 10000 Hz and 100000 Hz) displays nearly constant value (~ 0.01) of $\tan(\delta)$ upto 150 K irrespective of the applied frequency. At higher temperatures, $\tan(\delta)$ shows frequency dispersion, which is due to the dipolar relaxation as a result of B-site disorders. At room temperature, GCTO has a moderate dielectric constant (~ 191) and low dielectric loss (~ 0.42) at 100 Hz which makes it useful for room temperature dielectric application. Along with that robust dielectric response with respect to temperature and frequency makes it a promising dielectric metamaterial for miniaturization in microelectronic device applications.

Investigation of the magnetic ground state of double perovskites having transition metal ions at A and B sites is quite interesting, here we have investigated the magnetic properties of GCTO. Molar magnetic susceptibility (χ) plots (Figure 4(a)) measured in zero field cooled (ZFC) and field cooled (FC) modes from room temperature down to 4 K under the application of 1 Tesla applied magnetic field are exactly superimposed on each other and indicates paramagnetic nature of GCTO. Random distribution of Cu^{2+} and Ti^{4+} ions over B-site suppresses magnetic ordering in GCTO down to 4 K. Further paramagnetic property is investigated using Curie Weiss (CW) fitting (shown in the inset of Figure 4(a)). From the slope and intercept of the CW fit, effective magnetic moment, $\mu_{\text{eff, expt}}$ is evaluated. The CW temperature (T_{CW}) and effective magnetic moment $\mu_{\text{eff, expt}}$ are 3.5 K, $11.5 \mu\text{B}$ respectively. The resultant theoretical effective magnetic moments for the magnetic ions (Gd^{3+} and Cu^{2+}) present in GCTO is $11.3 \mu\text{B}$, which agrees well with the experimental value of $11.5 \mu\text{B}$. In order to determine the influence of magnetic field on exchange interactions among the magnetic spins present in GCTO, isothermal magnetization measurements ($M(H)$) were performed from 4 K to 50 K in magnetic fields from 0 T to +7 T (Figure 4(b)) and from -7 T to +7 T (inset of Figure 4(b)). S-type behaviour of $M(H)$ curve at 4 K tending to saturate at 7 T with a high value of magnetization ($13.25 \mu\text{B}/\text{f.u.}$) and the low remnant magnetization value ($0.015 \mu\text{B}/\text{f.u.}$) together with 35 Oe coercive field indicating soft ferromagnetic behavior. This

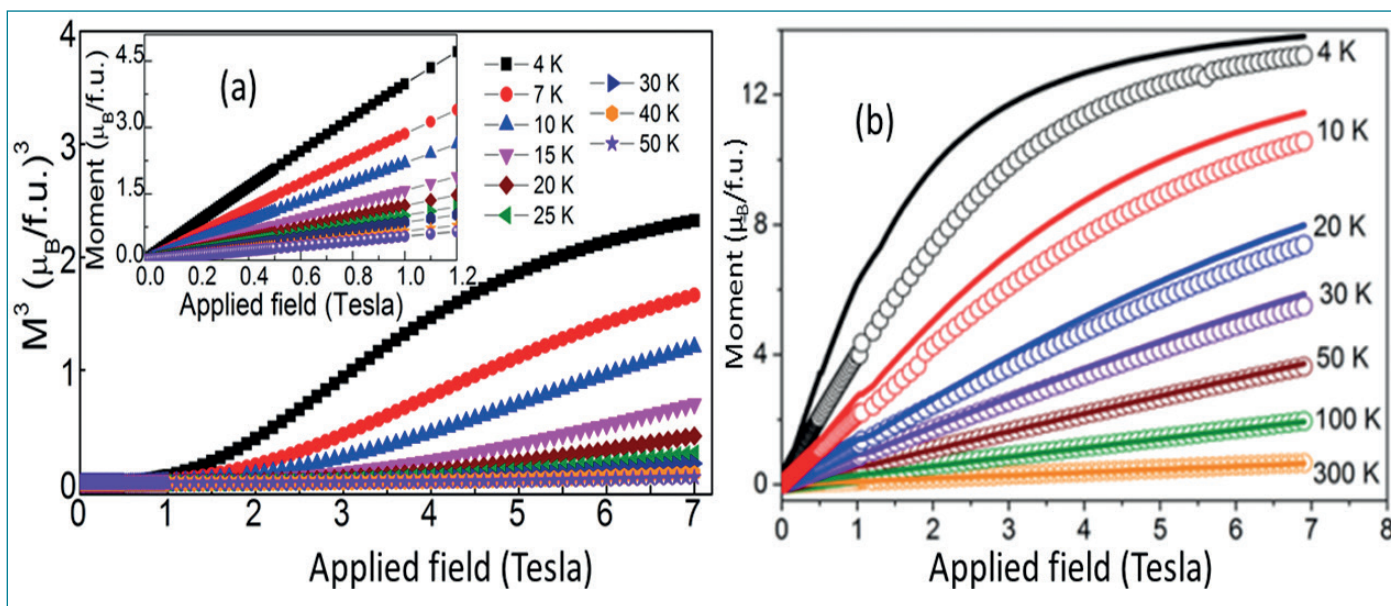


Figure 5. (a) Arrott plots M^3 vs. H plots, Inset: $M(H)$ curves upto 1.2 T applied field exhibits linearity. (b) $M(H)$ curves fitted using Brillouin function at several temperatures, symbols signifying the observed pattern and solid lines are the calculated magnetization values using Brillouin function.

demonstrates the presence of a weak ferromagnetism in GCTO. The higher value of saturation magnetization ($13.25 \mu_B/f.u.$) at 4 K indicates the contribution due to the magnetic correlations involving nearest neighbor interactions among the 4f spins of Gd^{3+} ions is larger than the other interactions viz., $Gd^{3+}-Cu^{2+}$ and $Cu^{2+}-Cu^{2+}$ spins via oxygen ions. While with increasing temperature, thermal energy weakens the ferromagnetic exchange interactions among the neighboring spins giving rise to the overall reduced magnetization.

$M(H)$ curves exhibit linear nature with the applied magnetic field in the range of 0 T to 1.2 T (inset of Figure 5(a)) and deviate from linearity at higher fields (Figure 4(a)). The non-hysteretic and linear variation of $M(H)$ curves indicates the paramagnetic nature. Magnetization curves were further examined for the possible exchange interactions with rising thermal energy from the field dependence of the magnetization, M^3 vs H plots or Arrott plot (Figure 5(a)). From Figure 5(a) below 10 K downward positive curvature and above 10 K upward positive curvature is noticed. This indicates that there are short range FM correlations around 10 K. The isothermal magnetization data were further analyzed using Brillouin function and the calculated magnetization pattern using this function is shown by line in Figure 5(b). The calculated data matched well with the experimental data (shown by symbol) in Figure 5(b) from room temperature down to 20 K. Below 20 K, deviation is observed and with the decrease in temperature deviation increases indicates the presence of short-range ferromagnetic correlations in GCTO.

Investigation on the optical properties of GCTO is noteworthy. Pseudo-absorption is calculated using Kubelka-Munk function ($F(R)$) from the

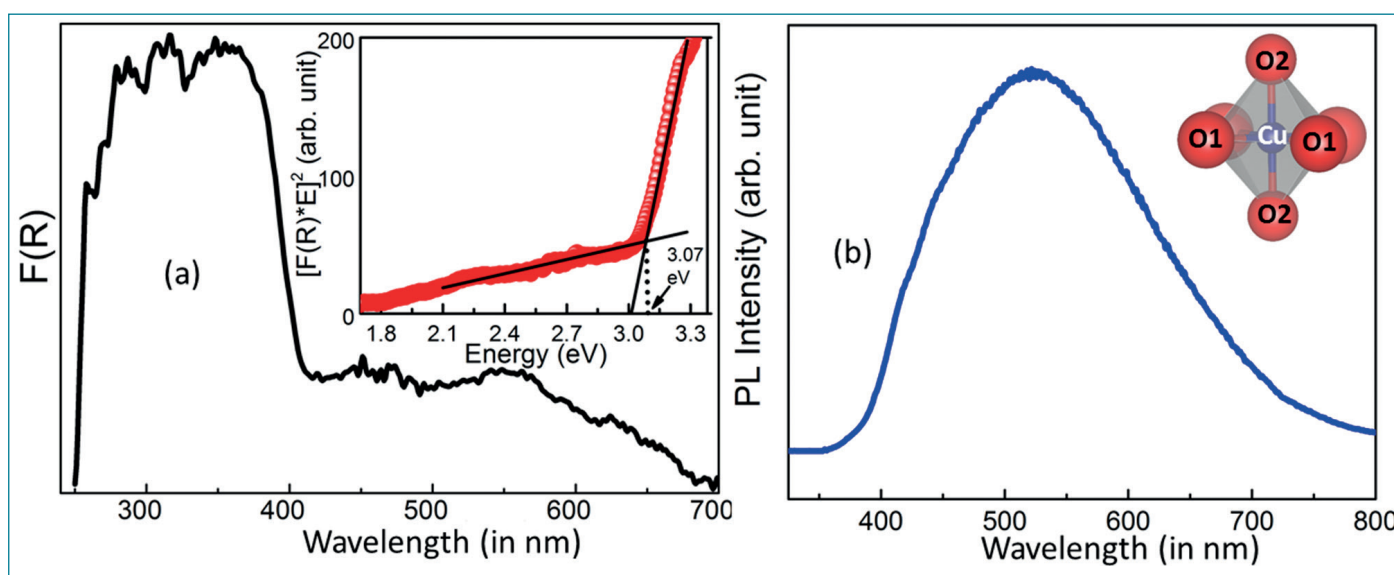


Figure 6 (a) Kubelka-Munk function, $F(R)$ plotted against wavelength shows optical absorption in the UV-visible region. Inset: Tauc plot $[F(R) \cdot E]^2$ vs. E (b) room temperature photoluminescence emission spectrum, inset: Cu-O6 octahedra.



diffuse reflectance data which is shown in Figure 6 (a). Significant absorption (Figure 6(a)) is observed in the UV-Vis region by GCTO. In this compound, the valence band is filled with 2p orbitals associated with oxygen ions, while the conduction band comprises 3d orbitals from Cu and Ti ions. The absorption from 250 nm to 410 nm is attributed to the charge transfer band (CTB), specifically the transition of $Ti^{4+}-O^{2-}$. The lower-intensity absorption in the longer wavelength region attributed to the presence of transition metal ions and d-d transitions which involve the unfilled d-orbitals of Cu^{2+} ions, as well as d-p transitions. Further the direct band gap (3.07 eV) of GCTO is calculated using Tauc plot (inset of Figure 6(a)). The high absorption capability of GCTO with wide bandgap in the UV-visible range suggests that this material could be a promising candidate for photocatalytic applications. The photoluminescence excitation spectrum of GCTO reveals maximum excitation intensity around 360 nm and further to see the charge carrier recombination process, GCTO is excited using 355 nm LASER source. Significant photoluminescence emission (PL) is observed in the visible region and the band gap obtained from PL spectrum is 2.37 eV. This lower value of the band gap from the PL spectrum compare to band gap obtained from Tauc plot using the diffuse reflectance data suggests the presence of intermediate energy bands in GCTO. Particularly, Cu^{2+} ions coordinated with oxygen in a six-fold geometry (shown in inset of Figure 6(b)), acts as an active PL emissive centre here. Indeed GCTO characterized by its high thermal stability (not shown here) and its ability to absorb and emit light over a wide range in the visible region can be considered as a potential candidate for light harvesting devices and other applications, including photovoltaic and optoelectronic devices.



Dr. Cherian K. Mathews founder of the Chemistry program at IGCAR passed away on April 9, 2024 at the age of 89. He pursued his graduation from Union Christian College, Aluva and his post-graduation from St. John's College, Agra. In 1959, after completing a one-year training program, he joined the Radiochemistry Division at Bhabha Atomic Research Centre (BARC). Later, he obtained his doctoral degree from McMaster University in Ontario, Canada. In 1970, he was identified to establish a Radiochemistry Laboratory (RCL) at IGCAR, Kalpakkam (the then Reactor Research Centre). Under his leadership, Radiochemistry laboratory at IGCAR was designed, constructed, commissioned, and made operational in 1980.

As an able administrator, Dr. C.K. Mathews spearheaded the transformation of the IGCAR Central Library into a digital resource as Chairman of the Library Committee.

His intense and intellectual vision perceived the role of chemistry in every aspect of the Fast Breeder Reactor Program, and his versatility enabled him to develop a variety of world-class facilities and research programs at IGCAR. The Centre is forever indebted to him for his pioneering contributions and for nurturing excellence in every activity.

In the passing away of Dr. C. K. Mathews, the country lost a renowned scientist who made pioneering contributions to the nation's fast reactor program, an exceptional administrator, and an innovative entrepreneur.

Editorial Team

News and Events



Technology Transfers Facilitated by Incubation Centre, IGCAR

January - February 2024

Three matured IGCAR technologies, developed to meet the Atma Nirbhar Bharat goals of our government were transferred to three different start-ups/industries during January-February'2024:

(i) Pulsating Sensor based Conductivity Meter is a high performance instrument developed at EIG, IGCAR using a new class of sensors, namely pulsating sensors. Unlike conventional instruments this meter works entirely in digital domain. The meter is capable of measuring conductivity of aqueous solutions over a broad range from 60 nS/cm to 1 S/cm (accuracy better than +/- 2% full scale) and displays the normalized conductivity at 25°C and at ambient temperature. This unit is compact and pipeline mountable for real-time measurement in plants or offline laboratory applications according to the user requirement. The unit can be interfaced through communication ports to PC or laptop for continuous logging of data for further analysis. It has been benchmarked with a standard unit. Performance of this device has been validated with many applications in IGCAR and found to be robust even in demanding environments. This technology was transferred on 04.January.2024 to a Bengaluru based start-up that wants to develop this technology for use in agricultural sector.

(ii) The Autonomous Gamma Dose Logger (AGDL) is a radiation monitor developed at SQRMG, IGCAR to measure environmental radiation in a wide range from 100 nGy/hr to 5 Gy/hr. The AGDL uses Geiger-Muller tubes to measure the environmental gamma dose rate. It transmits the data through wireless communication and backs up the data in a portable data logger. This system can be used for both routine and emergency radiation field monitoring purposes in nuclear installations and as a general environmental radiation monitoring equipment in other places. This technology was transferred to a Mumbai industry on 13th February, 2024. Dr.



IGCAR's Autonomous Gamma Dose Logger technology was transferred to a Mumbai industry on 13th February, 2024. Dr. N. Subramanian, Head, Incubation Centre, IGCAR handed over the technology license to the industry, while Dr. C. V. Srinivas, Head, EAD handed over the know-how document. The event was attended by senior scientists, technology developers and representative from the industry.



Pulsating Sensor based Conductivity Meter technology, developed at EIG, IGCAR, was transferred to a Bangalore start-up on 4th January, 2024. The event, arranged by Incubation Centre-IGCAR was attended by senior scientists, technology developers and representatives from the start-up.

Technology Transfer of HEPA Filter Test Rig (4th January, 2024)



The HEPA Filter Test Rig facility developed at SQRMG, IGCAR is currently operating as a NABL Certified Laboratory for testing/certifying HEPA filters. This test rig technology know-how was transferred to a Nagarcoil start-up that specializes in HEPA filters on 04th January, 2024. The technology transfer license documents were handed over by Dr. N. Subramanian, Head, IC-IGCAR to the licensee industry in the presence of by senior scientists and the technology developers team.

N. Subramanian, Head, Incubation Centre, IGCAR handed over the technology license to the industry, while Dr. C. V. Srinivas, Head, EAD handed over the know-how document. The event was attended by senior scientists, technology developers and representative from the industry.

(iii) The High Efficiency Particulate Filter (HEPA) Test Rig Facility, developed at SQRMG, is meant for testing HEPA Filter Assemblies having 610 x 610 x 290 mm dimension. The system consists of a wind tunnel for making uniform mixing of aerosols in the upstream, expander sections for mounting filter assembly on both upstream and downstream side, a pneumatic system for holding filter assembly with leak tight, wind tunnel with blower system in the downstream. The test rig is designed as per British Standard BS2831 which is now modified with latest version. In particular, it is a tailor made unit for HEPA filter assembly testing. The dimension of the upstream side wind tunnel and expander section are very crucial for the uniform mixing of challenge aerosols and face velocity. The location of the sampling ports and isokinetic sampling of challenge aerosols are critical aspect in the design of test rig for effectiveness in evaluation filter assembly. This Test rig facility at IGCAR is operational as a NABL Certified Laboratory. This technology was transferred on 4th January, 2024 to a Nagarcoil industry that specialises in manufacturing air filters

Reported by
Dr. N. Subramanian
Head, Incubation Centre



Workshop on Electromagnetic Nondestructive Evaluation

March 4-6, 2024

Workshop on Electromagnetic Nondestructive Evaluation (ENDE) is a series of conferences held annually in different parts of the world. The 27th in the series was conducted in India after a long gap of 12 years during March 4-6, 2024 in Ideal Beach Resort, Mamallapuram by Indira Gandhi Centre for Atomic Research. The inaugural function of the event was held on 4th March 2024



Releasing of the souvenir in the inaugural function of ENDE-2024

and was presided over by Shri S. Raghupathy, RRF & Former Director, Reactor Development and Technology Group, IGCAR. Dr. Komal Kapoor, Chief Executive, Nuclear Fuel Complex (NFC), Hyderabad was the Chief Guest, Shri P. A. Suresh Babu, Director-HR, Nuclear Power Corporation of India Ltd., Mumbai and Shri B. Saravanan, Director, Atomic Minerals Directorate, Hyderabad were the Guests of Honour. A souvenir containing essential information of the conference was released during the inaugural function.

The technical programme of the conference consisted of 4 plenary lectures (two sessions), 6 keynote lectures and presentations of 34 contributory papers. All keynote lectures and contributory presentations were scheduled in 8 different sessions having different themes of ENDE such as Modelling and Simulation, Material Characterization, Nuclear Applications, Inverse Problems and Image Processing, Industrial Applications, Advanced ENDE Sensors & Novel applications and Microwave and Terra Hertz Imaging. A total of 75 delegates from R&D sectors, industry and academia participated and presented papers including seven papers from foreign delegates. A few selected papers presented during the conference are being reviewed for publication in the International Journal of Applied Electromagnetic and Mechanics by SAGE publishers (formerly IOS Press). The participants were immensely benefited by way of interactions with eminent experts from abroad and India.

Reported by
Dr. Anish Kumar
Metallurgy and Materials Group



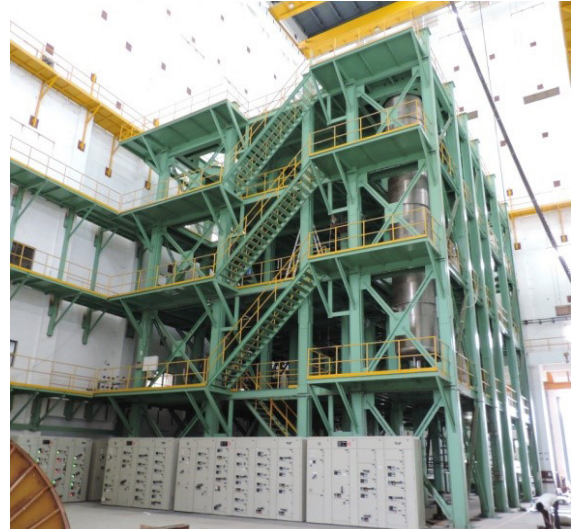
Sodium Charging in Sodium Technology Complex

May 10, 2024

The Sodium Technology Complex (STC) is set-up to support the various R&D activities on sodium technology for future FBRs. It is located on the south-west part of newly developing IGCAR North site. It houses a large sodium test rig augmenting the number of sodium facilities in the Fast Reactor Technology Group (FRTG).

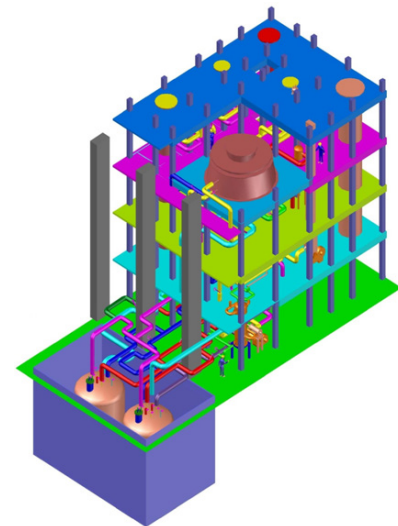
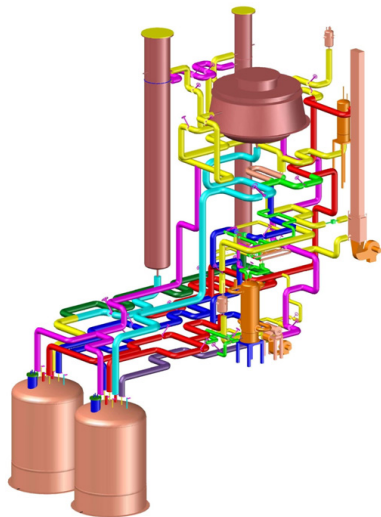


Exterior view of STC



Steel Structure with test vessels

The various experimental studies conceived in sodium technology complex are - the development & testing of critical reactor components, integral testing of reactor systems under simulated operating conditions, development & testing of sodium instrumentation, modal testing of full-scale reactor components, development and qualification of in-service inspection techniques for FBRs, heat & mass transfer studies of large diameter sodium pool and technology development for sodium cleaning.



3D model of STC components & sodium piping

The civil building of the sodium technology complex is of 40 m length and 21 m width. The total height of the engineering hall is 43 m, and it is provided with two EOT cranes of 25 tonnes and 10 tonnes capacity. The complex is compartmentalised as sodium rig area, components air testing area, clean room, material storage bay, an automated in-house sodium cleaning setup and a sodium disposal facility. The layout of the complex is optimised for the space utilisation, movement of sodium wetted components and ease of handling various components. Future expansion requirements of the complex are also taken into consideration.



Sodium Piping of STC

The heart of the complex is the sodium test rig which consists of three sodium vessels, associated sodium piping and auxiliary systems. Three separate sodium test vessels were designed to satisfy the more general testing requirements. Sodium test vessel-1 (STV-1) and Sodium test vessel-2 (STV-2) with respective diameters of 1 m and 1.5 m and a length of 13.8 m facilitate in-sodium testing of long slender mechanisms, sodium level sensors, passive safety devices etc. Sodium test vessel-3 (4.5 m dia. and assembled height also of 4.5 m) is planned to be used for the development of under sodium viewing systems, heat & mass transfer studies in argon cover gas etc. The total sodium inventory of the facility is 100 tonnes.

All the components of the sodium test rig are designed as per ASME Sec VIII, Div. 1, with maximum operating temperature of 600°C; STV-2 is designed for operating at 650°C (max.). The sodium piping is designed as per ASME B 31.1 code. The material of construction is SS 316 L(N). The test rig and the support structure are qualified for maximum credible seismic events as well as for most severe cyclonic condition.



The then Director of IGCAR, Dr. B. Venkatraman in the presence of Smt. Nidhi Tewari, Deputy Secretary, PMO inaugurated first charging of Sodium in Storage tank of STC

Detailed safety reviews at all stages of construction and commissioning have ensured a safe working environment. A significant achievement in May 2024 was the commencement of sodium charging, starting with an initial transfer of 4 tonnes of sodium. The activity was inaugurated by the then Director, IGCAR, Dr. B. Venkatraman in the presence of Smt. Nidhi Tewari, Deputy Secretary, PMO. It is planned to complete sodium charging and commission the facility by mid-2025.

Reported by
Dr. B.K. Sreedhar and colleagues
Fast Reactor Technology Group



Theme Meeting: Radiation Metrology and National Standards for Ionising Radiation May 21-22, 2024

A two-day theme meeting on "Radiation Metrology and National Standards for Ionising Radiation" (RM-NSIR-2024) was held during May 21-22, 2024 at IGCAR, Kalpakkam; This meet was organised by IGCAR in association with Metrological Society of India (MSI), & Indian Association for Radiation Protection (IARP). Shri. D. K. Shukla, Chairman, AERB was the Chief guest, Dr. D. K. Aswal, Director, HSEG, BARC and Dr. M. S. Kulkarni, Head, Health Physics Division, BARC were the guests of honor, Dr.



B. Venkatraman, the then Director, IGCAR delivered the presidential address. The theme meeting included Invited talks by eminent

speakers of national and international repute in the field of metrology, radiation standards, type testing, calibration of radiation measuring instruments, traceability of measurements, facts and misconception of radiations risk and a panel discussion. Nearly 60 delegates from BARC, IGCAR, AERB, NPCIL and Medical Centers & Industry participated in the meeting. This meeting had participation from eminent experts in the field facilitating robust interactions with state-of-the-art metrological facilities that have been commissioned at IGCAR.



Reported by
Smt. M. Menaka
Radiological Applications & Technology Division
Safety, Quality & Resource Management Group



Inauguration of Facilities by Dr. A. K. Mohanty, Chairman, AEC & Secretary, DAE

28th May, 2024

A facility 'Sub-assembly level Metal Fuel Fabrication Facility' was setup for fabrication of sodium bonded metal fuel pins of 1 meter length at Radiochemistry Laboratory, MC&MFCG. The facility will cater to sub assembly level irradiation program of metallic fuel pins of various designs in FBTR for target burn-ups. The facility has a design capacity to produce one fuel pin per day. The scaled up facility was designed based on experience gained on the process flow sheet developed by IGCAR and BARC. It consists of a high purity inert atmosphere glove box train which houses various process equipments with unique automation systems. The negative pressure and purity in the glove boxes are maintained by a SCADA/HMI based PLC controlled feed-bleed system. The automatic pressure control takes care of normal and emergency ventilation situations by means of pressure regulators and pneumatic valves. The glove boxes house alloy receipt and processing unit, weighing machine, cutting and aliquot preparation machine, alloy making and compact injection casting system with fixed material handling mechanism, de-moulding and end-shearing machine, machine vision based slug inspection bench, slug settling-cum-sodium bonding furnace, end plug welding machine, post-weld heat treatment furnace, helium leak testing chamber and decontamination chamber. The pin fabrication facility also encompasses laser marking machine, automatic



Inauguration of Sub-assembly level Metal Fuel Fabrication Facility



Inauguration of experimental facility for demonstration of unit operations of pyroprocessing

wire wrapping machine, sub-assembly construction station and inspection jig. The glove box train was commissioned by qualification of all process equipments and operating the glove box inert gas recirculation and purification system. This facility was inaugurated by Dr. A. K. Mohanty, Chairman, AEC & Secretary, DAE in the presence of Dr. B. Venkatraman, Director, IGCAR on 28th May 2024.

A new experimental facility for demonstrating unit operations of pyroprocessing by using U-Pu-Zr alloy in 250 g (maximum) per batch was setup at Radiochemistry Laboratory, MC&MFCG. The experimental facility will be used to generate data on the electrodeposition characteristics of uranium and plutonium from U-Pu-Zr as anode and to consolidate them further using vacuum salt and cadmium distillation followed up by induction melting. The design of high temperature process vessels was based on the group's vast experience on pyroprocessing of uranium based alloys in laboratory and 1 kg scale. This facility consists of two glove box trains operated under inert atmosphere. Pressure control system, solenoid valves and butterfly valves maintains the glove box train pressure within -20 to -40 mm of water column. A gas analyser station analyses trace moisture, trace oxygen and percentage level of nitrogen in argon sampled from glove box train. Pressure drop across glove box's HEPA filters is monitored continuously. The glove box also houses weighing modules and other utilities for preparation of LiCl-KCl eutectic containing UCl_3 with a view to load them in crucible, electro refining cell and in vacuum distillation cell for removing occluded salt and alloyed cadmium from cathode deposit. The glove boxes have other process utilities such as high resolution digital panel meters, graphical temperature data recorders, etc. for monitoring various process parameters during operations. The glove box train, purification and argon piping system were tested and qualified & commissioned. The facility was inaugurated by Dr. A. K. Mohanty, Chairman, AEC & Secretary, DAE in the presence of Dr. B. Venkatraman, Director, IGCAR on 28th May 2024.

Reported by
Dr. V. Jayaraman,
Materials Chemistry & Metal Fuel Cycle Group



Signing of MoU between IGCAR and M/s. Sree Maruthi Marine Industries Limited

7th June, 2024

The 2 Million Imperial Gallons per Day (380 m³/h) capacity Sea Water Reverse Osmosis (SWRO) desalination plant at IGCAR has been operating continuously since December 2015, playing a crucial role in providing potable water for DAE facilities in Kalpakkam conforming to IS 10500. It processes 1100 m³/h of seawater with Total Dissolved Solids (TDS) ranging from 30000 ppm to 36000 ppm received from the Auxiliary Seawater System (ASW) of BHAVINI.

Currently, the plant generates a reject stream of about 700 m³/h, containing brine with TDS ranging from 50000 ppm to 64000 ppm. This brine is discharged into the PFBR condenser outfall canal with a specialized diffuser arrangement, ensuring that it is diluted before reaching the sea.



Signing of MoU between IGCAR and M/s. Sree Maruthi Marine Industries Limited

Recognizing the potential value of the high TDS brine, efforts are undertaken to utilize it for industrial salt production instead of direct discharge into the sea.

A Memorandum of Understanding (MoU) was signed on 07.06.2024 between IGCAR and M/s. Sree Maruthi Marine Industries Limited, who is operating a salt manufacturing unit at Manamai (with TIDCO having a 33% stake), to redirect the reject brine to their salt pans approximately 5 km away from the desalination plant.

The project involves laying a new pipeline: the section from the desalination plant to the IGCAR compound wall (near Watch Tower-4), about 1.2 km in length, will be installed by the department. The remaining section, extending from the IGCAR compound wall to the salt pans outside the campus, will be constructed by M/s. Sree Maruthi Marine Industries Limited.

This initiative enhances cleaner salt production yields compared to seawater, ensures environmentally responsible disposal of brine, contributing to sustainable resource management in the region and creates job opportunity.

Reported by:
Biswanath Sen
Engineering Service Group



Workshop on Geospatial and Radar Technologies for Improved Weather Modelling and Effective Disaster Management (GRADM 2024), IGCAR, Kalpakkam

12-14 June, 2024

A three-day thematic workshop on "Geospatial and Radar Technologies for improved weather modelling and Disaster Management (GRADM-2024)" was held during 12-14 June, 2024 at IGCAR, Kalpakkam. The workshop was organized by IGCAR in association with National Remote Sensing Centre (NRSC), Hyderabad and Indian Association for Radiation Protection, Kalpakkam chapter



Inaugural Session of GRADM - 2024



Dr. R. Divakar, Acting Director & Director MMG, delivering the presidential address



Chief Guest Dr. S.K.Srivastava, Chief General Manager, RRSSC-NRSC & Keynote Speaker-1



Prof V. Chandrasekar, CSU, USA Guest of Honour & Keynote Speaker-2



Dr V. Srinivasa Prasad, Head NCMRWF, Guest of Honour and Invited Speaker

(IARP-K). Sri S.K.Srivastav, Outstanding Scientist and Chief General Manager, NRSC was the chief guest and Prof V.Chandrasekar, University Distinguished Professor, & Director of CSU CHILL, USA and Dr. V.Srinivasa Prasad Head, NCMRWF, New Delhi were the Guests of Honour. Dr. R.Divakar, the then Acting Director, IGCAR and Director MMG delivered the presidential address. The workshop comprised eight technical sessions with invited & contributory talks covering different areas : Geospatial Technologies in Disaster Management, Radars for Monitoring and Early Warning of Extreme Rainfall/ floods, Numerical Weather modelling of High Impact Weather Systems with Radar /Satellite observations , Meteor and Wind Profiler Radars in Atmospheric Studies and Ocean observations and modelling.



The workshop was attended by about 75 Scientists and Engineers from NRSC, NCMRWF, IMD, ISTRAC, NIOT, INCOIS, IGCAR, FAB-Govt of Kerala, AERB, NPCIL, Bhavini, Five Professors from CSU, USA; King Abdullah University of Science and Technology (KAUST), Thuwal, Saudi Arabia; Anna University, Chennai; Sri Venkateswara Univ., Tirupati; and Satyabama University Chennai, besides research scholars and students from different universities and representatives from different companies. The workshop provided sound interactions to evolve methodologies with advancements in geospatial technologies and Atmospheric Radars for numerical weather modelling, developing Decision Support systems towards effective disaster management and also to promote utilization of radars in scientific understanding of atmospheric phenomena.

Reported by
Dr. C. Venkata Srinivas,
Environmental Assessment Division,
Safety, Quality & Resource Management Group

Celebrating Nature at IGCAR: World Environment Day, 2024

June 5th, 2024

Indira Gandhi Centre for Atomic Research (IGCAR), celebrated World Environment Day, on June 5th, 2024 commemorating the institute's commitment to environmental sustainability. This year, in alignment with the theme of World Environment Day focusing on "Land Restoration, Desertification, and Drought Resilience," IGCAR included a meaningful tree-planting ceremony held at the premises of BARC training school- IGCAR campus.

The event was inaugurated by Shri C. G. Karhadkar, Director of IGCAR, who set the tone by planting a fruit tree. This symbolic gesture was followed enthusiastically by group directors, associate directors, scientists, researchers, and staff from various departments of IGCAR, who actively participated in planting a variety of native fruit trees like custard apple, jamun, jackfruit, and water-apple



Director, IGCAR planting a fruit tree

within the campus. This collective effort was seen as a significant step towards creating a greener and healthier ecosystem within the research facility.

Reported by
Dr. C. Venkata Srinivas,
Environmental Assessment Division,
Safety, Quality & Resource Management Group



Awards & Honours

- **Dr. Sandip Dhara** has been inducted as member of Board of Studies, Physics, SRM University, Chennai. He is also included as member of Editorial board member of Asian Journal of Physics, Indian Spectroscopy Society, Delhi, India and International Journal of Nuclear Materials, Technolock, inc.
- **Ms. B. R. Vaishnavi Krupa, Dr. Arup Dasgupta, Dr. Chanchal Ghosh and Dr. Shyam Kanta Sinha** received Certificate of appreciation from International Centre for Diffraction Data in recognition of contribution of 1 pattern to the Powder Diffraction File- Release 2025.
- **Indira Gandhi Centre for Atomic Research, Kalpakkam** has been awarded 3rd rank in recognition of the Swachhata activities undertaken by the unit as part of Swachhata Pakhwada (Feb. 2024).

Best Paper/Poster Award

- **Mr. S. Haribabu** received IIM Kalpakkam chapter - Best Journal paper for the year 2023-24, under Young researcher category for the article titled "Phase Selection and Microstructure Evolution in Laser Additive Manufactured Ni-Based Hardfacing Alloy Bush"; **S. HariBabu, C. Sudha, C.P Paul, V. Srihari, Alphy George, A. Dasgupta, K.S. Bindra**, Metall. Mater Trans A 55, (2024) 218–231
- **Ms. Ankita Pal** received IIM Kalpakkam chapter - Best Journal paper for the year 2023-24, under Young researcher category for the article titled "High-contrast corrosion mapping of dissimilar metal weld joints using alternating current scanning electrochemical microscopy: A case study with Zr-4—Ti-304L SS weld", **Ankita Pal, Nanda Gopala Krishna, A. Ravi Shankar and John Philip**, Corrosion Science 221 (2023) 111345.
- **Dr. Amit Kumar, Ms. Usha Pujala, Shri E. Hemanth Rao, Dr. V. Subramanian, Shri. Sanjay Kumar Das, Dr. D. Ponraju, and Dr. B. Venkatraman** secured the 'Best Platform Presentation' award at the Indian Aerosol Science and Technology Association (IASTA) National Conference 2023, held at Hotel Vivanta, Navi Mumbai, during 12 -14 December 2023 for the paper titled "Assessment of Fission Product and Sodium Aerosol Behavior in a closed chamber".
- **Ms. Sayani Mitra, Dr. Renjith Ramachandran and Dr. R. Rajaraman** received best poster awards for the poster titled "Computing positron lifetime and Doppler broadening parameters of structurally relaxed vacancies in Vanadium" in NPMMI-2024 (Nuclear Probes for Materials, Medicine and Industry - 2024) DAE-BRNS theme meeting held during 7th and 8th of June 2024 at Anushaktinagar, BARC.
- **Dr. Renjith Ramachandran, Dr. S. Balaji and Dr. K. Suresh** received best poster awards for the poster titled "Radiation damage studies on fusion first-wall materials using positron annihilation spectroscopy" in NPMMI-2024 theme meeting.
- **Ms. T. Sreepriya** received the "Best Poster Presentation Award" for the paper "Effect of thermal Aging on microstructure of Zr Added P9 Steel and correlation to nanomechanical Properties", **T Sreepriya, R. Mythili, Pooja Gupta, and S. K. Rai** at the International Conference on Electron Microscopy and XLII Annual Meeting of the Electron Microscope Society of India, EMSI 2024, IIT Bombay, 16-18th May 2024, Mumbai, India

Achievement in DAE sports

- For the first time, Team RAMESWARAM had won the Overall title at the XXXVIII DAE Sports & Cultural Meet-2023 Table Tennis at KAGS,KAIGA.
- In the Men & Women Team Event, the Rameswaram Team emerged as Runners. Winner up in Men's Singles & Doubles Event; Runner-Up in Women's Doubles Event.
- Team officials are MEN Team: **S. ChinnaThambi** (MSG), **Chandara Mouli Sharma** (EIG), **B. Pavitharan** (BARC), **Sumit Kumar** (MAPS) WOMEN Team: **P. Parimalam** (EIG), **S. Kapila** (ADMIN), **D. N. Sangeetha** (SQRMG), **S. Revathy** (FRTG) VETERAN MEN Team: **M. Karunakaran** (ESG), **J. Anandan** (SQRMG), **MVR.Srikanth**(NRB) VETERAN WOMEN Team: **Sundari Madasamy** (FRTG), **C.Valarmathi** (MAPS)

Editorial Committee
Members:

Shri J. Rajan,
Shri P. Vijaya Gopal,
Dr. R. Mythili,
Dr. N. R. Sanjay Kumar
Dr. C. V. S. Brahmananda Rao,
Shri M. Thangamani,
Shri G. Venkat Kishore,
Ms. Sujatha P. N,
Shri M. Rajendra Kumar,
Shri S. Kishore,
Shri Biswanath Sen,
Dr. N. Desigan,
&
Shri K. Varathan

Bio-diversity @ DAE Campus, Kalpakkam



Red-necked falcon

The red-necked falcon is a medium-sized, long-winged bird with a bright rufous crown and nape photographed inside IGCAR campus. The wings and upper parts are bluish grey and the tail has narrow bars. The legs, ceres and eyering are yellow. The sexes are similar except in size, males are smaller than females.